Published in final edited form as:

Sci Transl Med. 2021 November 17; 13(620): eabh0272. doi:10.1126/scitranslmed.abh0272.

Deleting DNMT3A in CAR T cells prevents exhaustion and enhances antitumor activity

Brooke Prinzing[1,†], **Caitlin C. Zebley**[1,2,3,4,†], **Christopher T. Petersen**[1,†,‡], **Yiping Fan**[5], **Alejandro Allo Anido**[1], **Zhongzhen Yi**[1], **Phuong Nguyen**[1], **Haley Houke**[1], **Matthew Bell**[1,4], **Dalia Haydar**[1], **Charmaine Brown**[2], **Shannon K. Boi**[2], **Shanta Alli**[2], **Jeremy Chase Crawford**[2], **Janice M. Riberdy**[1], **Jeoungeun J. Park**[1], **Sheng Zhou**[1], **Mireya Paulina Velasquez**[1], **Chris DeRenzo**[1], **Cicera R. Lazzarotto**[6], **Shengdar Q. Tsai**[6], **Peter Vogel**[7], **Shondra M. Pruett-Miller**[8], **Deanna M. Langfitt**[1], **Stephen Gottschalk**[1,*], **Ben Youngblood**[2,*], **Giedre Krenciute**[1,*]

[1]Department of Bone Marrow Transplantation and Cellular Therapy, St Jude Children's Research Hospital, Memphis, TN 38105, USA.

[2]Department of Immunology, St Jude Children's Research Hospital, Memphis, TN 38105, USA.

[3]Department of Oncology, St Jude Children's Research Hospital, Memphis, TN 38105, USA.

[4]Graduate School of Biomedical Sciences, St Jude Children's Research Hospital, Memphis, TN 38105, USA.

[5]Department of Bioinformatics, St Jude Children's Research Hospital, Memphis, TN 38105, USA.

[6]Department of Hematology, St Jude Children's Research Hospital, Memphis, TN 38105, USA.

[7]Department of Pathology, St Jude Children's Research Hospital, Memphis, TN 38105, USA.

[8]Department of Cell and Molecular Biology, St Jude Children's Research Hospital, Memphis, TN 38105, USA.

[*]Corresponding author. giedre.krenciute@stjude.org (G.K.); benjamin. youngblood@stjude.org (B.Y.); stephen.gottschalk@stjude.org (S.G.).

[‡]Present address: BlueBird Bio, Cambridge, MA 02142, USA.

[†]These authors contributed equally to this work.

Author contributions: B.P., C.C.Z., C.T.P., S.G., B.Y., and G.K. designed the study. B.P., C.C.Z., C.T.P., S.G., B.Y., G.K., Y.F., J.C.C., J.-E.P., and S.Z. developed methodologies. B.P., C.C.Z., C.T.P., A.A.A., Z.Y., H.H., M.B., D.H., C.B., S.B., S.A., J.-E.P., S.Z., and D.L. performed in vitro experiments. B.P., C.T.P., P.N., and J.R. performed in vivo experiments. C.C.Z., Y.F., and J.C.C. performed bioinformatic analyses. S.M.P.-M. performed guide RNA design and NGS sequencing. C.R.L. and S.Q.T. performed CHANGE-seq. P.V. performed histopathological analysis. M.P.V. and C.D. provided xenograft models. All authors contributed to data analysis and manuscript preparation.

Competing interests: B.P., C.C.Z., C.T.P., J.C.C., S.G., B.Y., and G.K. are co-inventors on patent applications in the fields of T cell or gene therapy for cancer. S.G. has consulted for Tessa Therapeutics, TIDAL, Catamaran Bio, Nektar, and Novartis within the last 2 years and is a Data and Safety Monitoring Board (DSMB) member of Immatics. B.Y. has a consulting agreement with ElevateBio. S.Q.T. is a member of the scientific advisory boards of KromaTiD and Twelve Bio. Patents related to this work are the following: Immune cells with dnmt3a gene modifications and methods related thereto (WO2017079642A1), DNMT3A knock-out and STAT5 activated genetically engineered T-cells (WO2020210365A1), T cell gene expression analysis for use in t cell therapies (WO2020/222987), and Dna methylation profiling for t-cell immunotherapy (WO2018/104909). C.R.L. and S.Q.T. are co-inventors on a patent describing CHANGE-seq (US10920272B2). All other authors declare that they have no competing interests.

Data and materials availability: All data associated with this study are present in the paper or the Supplementary Materials. Raw data can be found in data file S2. DNA sequencing data have been deposited to the Gene Expression Omnibus (GEO) under the accession no. GSE184568.

Abstract

Chimeric antigen receptor (CAR) T cell therapy is revolutionizing cancer immunotherapy for patients with B cell malignancies and is now being developed for solid tumors and chronic viral infections. Although clinical trials have demonstrated the curative potential of CAR T cell therapy, a substantial and well-established limitation is the heightened contraction and transient persistence of CAR T cells during prolonged antigen exposure. The underlying mechanism(s) for this dysfunctional state, often termed CAR T cell exhaustion, remains poorly defined. Here, we report that exhaustion of human CAR T cells occurs through an epigenetic repression of the T cell's multipotent developmental potential. Deletion of the de novo DNA methyltransferase 3 alpha (DNMT3A) in T cells expressing first- or second-generation CARs universally preserved the cells' ability to proliferate and mount an antitumor response during prolonged tumor exposure. The increased functionality of the exhaustion-resistant DNMT3A knockout CAR T cells was coupled to an up-regulation of interleukin-10, and genome-wide DNA methylation profiling defined an atlas of genes targeted for epigenetic silencing. This atlas provides a molecular definition of CAR T cell exhaustion, which includes many transcriptional regulators that limit the "stemness" of immune cells, including CD28, CCR7, TCF7, and LEF1. Last, we demonstrate that this epigenetically regulated multipotency program is firmly coupled to the clinical outcome of prior CAR T cell therapies. These data document the critical role epigenetic mechanisms play in limiting the fate potential of human T cells and provide a road map for leveraging this information for improving CAR T cell efficacy.

INTRODUCTION

Cellular immunotherapy with adoptively transferred chimeric antigen receptor (CAR)–modified T cells is an attractive approach to improve outcomes for patients with cancer. However, even for the most successful CAR T cell therapy (1), CD19-CAR T cell therapy for $CD19^+$ acute lymphoblastic leukemia (ALL), only 50% of patients have responses that last more than 1 year (2). Complete responses are much lower for $CD19^+$ chronic lymphocytic leukemia (CLL) (3), and only a few long-term survivors have been reported for CAR T cell therapies targeting solid tumor or brain tumor antigens such as human epidermal growth factor receptor 2 (HER2), mesothelin, carcinoembryonic antigen-related cell adhesion molecule 5 (CECAM5), disialoganglioside (GD2), epidermal growth factor receptor variant III (EGFRvIII), and interleukin-13 (IL-13) receptor subunit α 2 (IL13Rα2) (4–9). Thus, there is a great need to further enhance the efficacy of CAR T cells and identify underlying biological mechanisms that dictate an individual patient's responsiveness to such therapies.

Given that the therapeutic efficacy of CAR T cell approaches has been closely linked to the in vivo persistence of transferred T cells and to their sustained effector functions (8–10), a critical and universally agreed upon goal for the field is to identify the mechanism(s) that restricts CAR T cell survival and function. Several studies have reported that prolonged stimulation of CAR T cells results in a functional exhaustion of their antitumor properties and promotes a rapid contraction in their quantity (11, 12). These hallmarks suggest that CAR T cells have undergone the developmental process of exhaustion; however, a more refined definition for CAR T cell exhaustion is lacking. In model systems that have

established the concept of T cell exhaustion, it is now clear that this developmental state is epigenetically reinforced to maintain exhaustion-associated gene expression programs (13–17). Epigenetic modifications can provide a cell-intrinsic mechanism that enables memory T cells to retain acquired gene expression programs during their antigen-independent homeostasis, indicating that, once acquired, exhaustion-associated epigenetic programs can be long-lived (13, 15–23).

We have recently reported that conditional deletion of the DNA methyltransferase 3a [*Dnmt3a* conditional knockout (cKO)] in murine T cells responding to a murine chronic viral infection preserves their effector functions and prevents their acquisition of canonical exhaustion gene expression programs (15). Although this work demonstrates that DNA methylation is a critical regulator of exhaustion programming in murine model systems, it remains to be determined whether this mechanism plays a causal role in the reinforcement of human memory T cell fates and specifically whether it is, at least in part, responsible for exhaustion of human CAR T cells. To better define the role of epigenetic programming in the efficacy of CAR T cell therapy and determine the broader impact of epigenetic regulation on human memory T cell differentiation potential, we investigated the effect of DNMT3A deletion on the effector function and survival of human CAR T cells. Here, we report that blocking de novo methylation programming in human CAR T cells preserved their differentiation capacity, allowing for sustained proliferation and effector function in the setting of chronic antigen exposure. From these studies, we defined an epigenetic signature of human CAR T cell exhaustion and gained new insight into the efficacy of prior CAR T cell trials, laying a foundation for the rational design of T cell therapies that provide long-lived antitumor activity and immunological protection.

RESULTS

DNMT3A KO preserves CAR T cell proliferative capacity and effector functions during chronic antigen stimulation in vitro

To evaluate the effects of DNMT3A-mediated de novo methylation on CAR T cell function, we developed a CRISPR-Cas9–based method for generating DNMT3A KO CAR T cells (Fig. 1A and fig. S1A). Briefly, T cells were electroporated with Cas9–single-guide RNA (sgRNA) ribonucleoprotein (RNP) complexes (Fig. 1A) targeting the catalytic domain (exon 19) (24) of DNMT3A (guide 2; fig. S1B) or mCherry, which served as a control (Ctrl) followed by transduction with retroviral vectors encoding a CAR. This method resulted in highly efficient (Fig. 1B and fig. S1C) and stable (fig. S1D) KO of DNMT3A irrespective of CAR construct with no effect on CAR cell surface expression (fig. S2A) or phenotype (fig. S2B) and with limited off-target gene disruptions (fig. S3).

To determine whether there were functional differences between DNMT3A KO and Ctrl CAR T cells, we used a repeat stimulation assay (Fig. 1C) (25, 26), in which CAR T cells were counted and stimulated with fresh tumor cells (U373) in the presence of IL-15 every 7 days at an effector-to-target (E:T) ratio of 2:1 throughout the duration of the assay. For effectors, we used T cells expressing HER2-CARs (27), IL13Rα2-CARs (28), or ephrin type-A receptor 2 (EphA2)-CARs (29) with a CD28ζ endodomain (second-generation CARs) or HER2-CARs with a ζ endodomain (first-generation CAR). Regardless of the

CAR T cell population, DNMT3A KO CAR T cell expansion was significantly greater than Ctrl CAR T cells ($P < 0.01$) (Fig. 1, D and E), with an average difference of 1.3-fold after the first stimulation, 2.5-fold after the second stimulation, 6.4-fold after the third stimulation, and 22.6-fold after the fourth stimulation, respectively (Fig. 1E). The expansion of DNMT3A KO CAR T cells followed an exponential growth pattern to a significantly greater extent than Ctrl T cells [mean R^2 values of fitted growth curves ($n = 17$): 0.9374 versus 0.6856; $P < 0.05$; fig. S4A], and DNMT3A KO CAR T cells required significantly fewer stimulations to double than Ctrl T cells ($P < 0.01$; fig. S4B). DNMT3A KO CAR T cell expansion was strictly antigen dependent, because culturing DNMT3A KO CAR T cells without tumor cells for 7 days resulted in a mean 93.2% of dead/dying DNMT3A KO CAR T cells (Fig. 1F and fig. S5). In addition, deletion of DNMT3A did not enhance expansion of nontransduced (NT) T cells or CAR T cells in the presence of antigen-negative tumor cells, further demonstrating that improved expansion of DNMT3A KO CAR T cells required antigen-mediated activation (fig. S6). We next evaluated whether the increased expansion of DNMT3A KO CAR T cells was due to increased proliferation or decreased apoptosis. We assessed Ki67 expression 24 hours after the fourth stimulation with tumor cells and found that a greater proportion of DNMT3A KO CAR T cells were Ki67 positive in comparison to Ctrl CAR T cells (fig. S7A). To assess apoptosis in Ctrl and DNMT3A KO CAR T cells after the fourth antigen stimulation, we used LIVE/DEAD Aqua (LDA) and annexin V staining. Flow cytometric analyses showed no change in the proportion of apoptotic DNMT3A KO CAR T cells compared with Ctrl KO CAR T cells (fig. S7B). These results suggest that the enhanced expansion of DNMT3A KO CAR T cells is due to increased proliferation, not decreased apoptosis. To confirm that the observed benefit was DNMT3A specific, we validated our findings using additional DNMT3A-targeting guide RNAs, one that also targeted the catalytic domain in exon 19 (guide 3) and two that targeted exon 3 (guide 1 and guide 7) (fig. S8), and a second tumor cell line (LM7, positive for HER2 and EphA2) (fig. S9), performed cocultures without exogenous IL-15 (fig. S10), and performed gain-of-function studies, in which we expressed a KO- resistant DNMT3A with a mutated protospacer adjacent motif (PAM) sequence in DNMT3A KO CAR T cells (fig. S11). Last, we demonstrated that the enhanced expansion associated with deletion of DNMT3A also occurred in CAR T cells with a 41BB, CD27, or OX40 costimulatory domain (fig. S12).

Having demonstrated that DNMT3A KO CAR T cells have a preserved capacity to expand in the presence of sustained tumor exposure compared to Ctrl CAR T cells, we next assessed their ability to produce cytokines and quantified their cytolytic activity. DNMT3A KO and Ctrl HER2.ζ-, HER2.CD28ζ-, or IL13Rα2.CD28ζ-CAR T cells were cultured with U373 cells. After 24 hours, the concentration of T helper cell 1 (T_H1) [granulocyte-macrophage colony-stimulating factor (GM-CSF), interferon-γ (IFN-γ), tumor necrosis factor–α (TNF-α), and IL-2] and T_H2 (IL-4, IL-5, IL-6, IL-10, and IL-13) cytokines was determined by multiplex analysis (Fig. 2A). Comparison of Ctrl and DNMT3A KO CAR T cells after one round of stimulation revealed that all analyzed cytokines were secreted at similar concentrations, except IL-10, which was significantly higher in samples from DNMT3A KO CAR T cells ($P < 0.001$; Fig. 2A and fig. S13, A and B). The same analysis was performed after the fourth stimulation, further highlighting IL-10 as the only differentially expressed cytokine and suggesting a role for IL-10 signaling in CAR T cell survival (Fig. 2B). To

determine whether the observed increase in IL-10 depended on the costimulatory domain of the CAR, we repeated our analysis using EphA2-CAR T cells with a CD28, 41BB, CD27, or OX40 costimulatory domain. DNMT3A KO CAR T cells produced higher concentrations of IL-10 at both the first and fourth stimulation regardless of the costimulatory domain used (fig. S13C). The cytolytic capacity of Ctrl and DNMT3A KO CAR T cells was also determined at the first and fourth stimulation. DNMT3A KO allowed CAR T cells to retain the ability to kill target cells at later stimulations compared to Ctrl CAR T cells (Fig. 2C). Deletion of DNMT3A did not affect the antigen specificity of the CAR as IL13Rα2.CD28.ζ DNMT3A KO CAR T cells had minimal cytokine production or cytotoxicity against U373 IL13Rα2 KO tumor cells (fig. S14). The decrease in functionality of Ctrl CAR T cells was also mirrored by phenotypic analysis, showing that DNMT3A KO HER2.ζ-CAR T cells were significantly enriched for a central memory T cell (Tcm) phenotype ($CD45RO^+$ $CCR7^+$) ($P < 0.001$) and expressed lower amounts of T cell immunoglobulin and mucin domain-containing protein 3 (TIM3) relative to Ctrl CAR T cells after the fourth stimulation (fig. S15A). Collectively, our data demonstrate that deletion of DNMT3A preserves CAR T cell proliferative capacity and effector functions during extended in vitro tumor challenge.

DNMT3A KO CAR T cells retain a stem-like epigenetic program during prolonged stimulation

Having established that DNMT3A KO enhances CAR T cell expansion and effector function during prolonged antigen exposure, we next sought to characterize the cell-intrinsic properties responsible for these differences by performing whole-genome bisulfite sequencing (WGBS) methylation profiling of Ctrl and DNMT3A KO CAR T cells after the fourth tumor cell stimulation (Fig. 3A and fig. S15B). We focused our analyses on $CD8^+$ T cells because $CD8^+$ CAR T cells were highly enriched (>90%) after four rounds of stimulation (fig. S15B). We identified more than 1600 genes that had differentially methylated regions (DMRs) among Ctrl KO and DNMT3A KO CAR T cells at the 4-week time point. These DMRs were predominantly localized to gene bodies (fig. S16A). Among the DNMT3A-mediated DMRs, we observed a notable enrichment of genes encoding transcription factors [transcription factor 7 (TCF7) and lymphoid enhancer binding factor 1 (LEF1)] that have been previously reported to become repressed during T cell terminal differentiation (30–32). Ctrl KO CAR T cell promoter regions became fully methylated in contrast to DNMT3A KO CAR T cells (Fig. 3B and figs. S16 and S17). These findings were further validated at the protein level using flow cytometry, which showed a higher abundance of TCF7 and LEF1 expression in DNMT3A KO CAR T cells after chronic antigen stimulation (fig. S18). Further, thymocyte selection–associated high mobility group box (TOX), a transcription factor recently found to promote T cell exhaustion (33–35), was among the list of transcriptional regulators upstream of DNMT3A target genes (fig. S16). We also observed methylation of the CD28 promoter in Ctrl but not in DNMT3A KO CAR T cells, indicating that the Ctrl T cells were exhausted, because CD28 promoter methylation is a prominent feature of chronically stimulated $CD8^+$ T cells isolated from individuals living with HIV infection (Fig. 3C). In addition, the loci of several homing molecules, including *ITGAE*, *CCR7*, and *SELL*, also remained unmethylated in DNMT3A KO CAR T cells (figs. S17 and S18). Thus, the epigenetic programming of DNMT3A KO CAR T cells resembles the epigenetic signature of naïve or stem cell–like memory T cells (fig. S17),

providing a mechanistic link to the preserved proliferative capacity and effector function observed in the DNMT3A KO CAR T cells. To gain insight into the kinetics for acquisition of these programs, we performed WGBS before and after four daily stimulations with tumor cells. Although a small subset of DNMT3A-mediated DMRs, including those that occur in the *TCF7* and *LEF1* loci, were acquired within the first week of tumor exposure (fig. S19), most DNMT3A-mediated DMRs, including methylation of the CD28 promoter, were acquired after prolonged stimulation of CAR T cells.

To further explore the biological pathways engaged by DNMT3A, we performed a gene ontology (GO) analysis of the methylation datasets. This analysis revealed involvement of the T cell receptor (TCR) and β-catenin pathways (Fig. 3D). Further characterization of the biological pathways affected by DNMT3A-regulated genes revealed statistically enriched pathways ($P < 0.001$) associated with T cell effector differentiation, including TCR signaling, leukocyte migration, cytokine signaling, and apoptotic regulation (Fig. 3E). Ingenuity pathway analysis (IPA) of the DNMT3A- regulated genes indicated that they were coupled to TCR signaling, T_H1 and T_H2 activation, and costimulation through CD28 (Fig. 3F).

Given the apparent preservation of stem-like features among the DNMT3A KO CAR T cells, we sought to further interrogate their developmental potential. We recently used a machine learning approach to analyze our collection of human $CD8^+$ T cell WGBS datasets and identified 245 CpG sites throughout the genome whose methylation status can predict the multipotent capacity of human T cells (36). Using this normalized multipotency index (MPI), we found that DNMT3A KO CAR T cells are predicted to have greater developmental plasticity than the stem-like subset of human memory T cells (Tscm) (Fig. 3G). In contrast, Ctrl KO CAR T cells had a predicted MPI similar to short-lived effector memory T cells (Tem) (Fig. 3G). The progressive decline in effector function of CAR T cells experienced during chronic stimulation has been ascribed to the process of T cell exhaustion (37). DNMT3A-mediated de novo DNA methylation programming was previously demonstrated to be a critical regulator of murine T cell exhaustion (37). To compare murine and human DNMT3A-controlled epigenetic programs, we cross-referenced our published murine exhaustion DMR list with our newly identified human CAR T cell DNMT3A-mediated DMRs (Fig. 3H). We found that, among the 1043 DNMT3A-targeted genes in chronically stimulated human CAR T cells (data file S1), 337 were also specifically targeted by DNMT3A during murine T cell exhaustion (Fig. 3H). This enrichment for epigenetically regulated exhaustion-associated genes in our human CAR T cell dataset indicates that epigenetic imprinting of exhaustion programs is a conserved biological mechanism limiting T cell effector responses.

Last, to assess whether knocking out DNMT3A improves the developmental potential of the total pool of T cells or whether it preserves or selectively enriches for T cells that inherently have a heightened differentiation capacity, we performed a gene set enrichment analysis (GSEA) on DNMT3A-targeted genes and existing gene expression profiles from resting human naïve and memory $CD8^+$ T cell subsets (fig. S20A). DNMT3A-associated gene enrichment scores were most similar to memory T cell subsets in comparison to naïve T cells. We next proceeded to determine whether DNMT3A deletion results in selective

survival of a population of T cells by establishing DNMT3A KO CAR T cells from purified naïve or memory $CD8^+$ T cell subsets. We generated these cells by first sorting naïve/Tscm ($CD45RO^-$,$CCR7^+$) and memory ($CD45RO^+CCR7^-$; $CD45RO^+CCR7^+$; $CD45RO^-CCR7^-$) $CD8^+$ T cells (fig. S20B), followed by CAR transduction and DNMT3A KO. For all four donors, DNMT3A KO CAR T cells derived from the naïve/Tscm T cell subset showed robust expansion; however, expansion was variable from DNMT3A KO CAR T cells derived from memory T cells (fig. S20C). Thus, DNMT3A deletion promotes the selective survival of developmentally plastic $CD8^+$ T cells during chronic stimulation.

IL-10 promotes DNMT3A KO CAR T cell survival in the setting of chronic antigen exposure

From our in vitro chronic stimulation studies, we had identified IL-10 as the dominant differentially expressed cytokine produced by DNMT3A KO CAR T cells. To investigate whether IL-10 plays a causal role, we first established an IL-10 gene expression signature on the basis of the published gene expression profiles of human T cells cultured with or without IL-10. Cross-referencing this signature with our DNMT3A gene target list, we found an enrichment of genes that are coupled to IL-10 signaling among the DNMT3A target genes (fig. S21A). To determine the role of IL-10 in the context of DNMT3A KO, we generated HER2.ζ-CAR T cells in which either IL-10 or DNMT3A, or both [double KO (DKO)] were deleted by CRIPSRCas9 gene editing (Fig. 4A and fig. S21, B to F). Ctrl, DNMT3A KO, IL-10 KO, and DKO CAR T cells were stimulated weekly with U373 tumor cells in the presence of IL-15 with or without exogenous IL-10 (Fig. 4A), and the lack of IL-10 production by IL-10 KO and DKO CAR T cells was confirmed by enzyme-linked immunosorbent assay (ELISA) (Fig. 4B). Although DNMT3A KO CAR T cells had an expected proliferative advantage in comparison to Ctrl CAR T cells, this sustained proliferative capacity was diminished in DKO CAR T cells (Fig. 4, C and D). In the presence of IL-10, this difference was reversed, confirming that IL-10 supports proliferation of CAR T cells.

We next performed whole-genome methylation profiling to assess the epigenetic state of all four CAR T cell populations before the first and after the fourth stimulation with tumor cells. Principal components analysis (PCA) of whole-genome methylation profiles revealed that DNMT3A-deficient (DNMT3A KO, DKO) and DNMT3A-intact (Ctrl, IL-10 KO) CAR T cell populations formed distinct clusters (fig. S22). Consistent with our previous findings, DNMT3A-mediated methylation of the stem-associated genes, *TCF7* and *LEF1*, occurred early in contrast to acquisition of methylation at other loci, including *CD28* (fig. S23). Likewise, DNMT3A KO CAR T cells retained a high methylation-based MPI in contrast to Ctrl CAR T cells (Fig. 4E). Consistent with the PCA, the DMRs were highly conserved between DNMT3A KO versus IL-10 KO and DKO versus IL-10 KO CAR T cells (Fig. 4F). Shared DMRs included aforementioned genes regulating T cell stemness such as *TCF7*, *LEF1*, and *CD28* (Fig. 4G and fig. S23). However, GO analysis also highlighted differences between DNMT3A KO and DKO DMR lists, including costimulation (Fig. 4H). Together with our observation that exhaustion-associated CD28 promotor methylation occurred in Ctrl but not DNMT3A KO CAR T cells, these data support a model in which IL-10 signaling serves as a negative feedback loop to limit CD28 costimulation in the setting of chronic antigen exposure.

DNMT3A deletion enhances the therapeutic efficacy of CAR T cells in preclinical solid tumor models

Next, we evaluated the impact of DNMT3A KO on the antitumor activity of T cells expressing EphA2.CD28ζ-, HER2.ζ-, or IL13Rα2. CD28α-CARs in vivo. We validated CAR expression and DNMT3A KO for each CAR T cell population used in the in vivo solid tumor studies (fig. S24). We first compared the antitumor activity of Ctrl and DNMT3A KO EphA2-CAR T cells in an intraperitoneal locoregional osteosarcoma (LM7) model. Gene-edited EphA2-CAR T cells were injected into LM7.GFPffLuc-bearing NOD-*scid* IL2Rgamma^{null} (NSG) mice. Whereas Ctrl and DNMT3A KO EphA2-CAR T cells both initially had potent antitumor activity, only DNMT3A KO CAR T cells maintained tumor control, resulting in a significant survival advantage ($P < 0.05$; Fig. 5, A to C). To investigate whether superior tumor control correlated with a less differentiated state of DNMT3A KO EphA2-CAR T cells in vivo, Ctrl and DNMT3A KO CAR T cells were purified using fluorescence-activated cell sorting (FACS) from tumor-bearing mice 1 week after injection and subjected to whole-genome methylation profiling (fig. S25, A and B). DNMT3A KO CAR T cells had a higher MPI score compared to the Ctrl CAR T cells, providing evidence for retained developmental plasticity (fig. S25C). Further, GO analysis of the DMR list highlighted the β-catenin–TCF complex, consistent with results from our in vitro studies (fig. S25, D to F).

We next evaluated DNMT3A KO HER2.ζ-CAR T cells in vivo in an intravenous lung-disseminated osteosarcoma model (26). On day 28 after LM7.GFPffLuc intravenous injection, mice received a single intravenous dose of Ctrl or DNMT3A KO HER2.ζ-CAR T cells. Whereas tumors progressed in Ctrl CAR T cell–treated mice, 5 of 10 mice treated with DNMT3A KO HER2.ζ-CAR T cells had a complete response, resulting in a significant survival advantage ($P < 0.01$; Fig. 5, D to F). Last, we examined the benefit of DNMT3A KO in CAR T cells targeting glioma. The antitumor activity of these glioma-specific CAR T cells had already been optimized by expressing IL-15 (IL13Rα2-CAR/IL-15) (25). U373.eGFP.ffLuc brain tumor–bearing NSG mice received one intratumoral injection of Ctrl or DNMT3A KO IL13Rα2-CAR/IL-15 T cells 7 days after tumor cell injection (Fig. 5, G and H, and fig. S26A). Mice treated with DNMT3A KO CAR T cells had a median survival advantage of 33 days in comparison to mice treated with Ctrl CAR T cells (DNMT3A KO: 117 days; Ctrl: 84 days). Although DNMT3A KO CAR T cell treatment did not extend survival relative to Ctrl CAR T cells (Fig. 5I), tumors in mice treated with DNMT3A KO CAR T cells grew significantly slower after initial progression as judged by bioluminescence imaging ($P < 0.05$; fig. S26B). In addition, histological examination of tumors demonstrated a greater T cell infiltrate in tumors treated with DNMT3A KO CAR T cells relative to Ctrl CAR T cells (fig. S26, C and D). Last, one antigen loss variant was observed (fig. S26E) after DNMT3A KO CAR T cell therapy. This finding suggests that, in addition to increasing T cell effector function, targeting multiple antigens as reported by us and other investigators (8, 9, 25) will be critical to improve clinical outcomes of CAR T cell therapy.

DNMT3A-mediated gene expression programs regulate CD19-CAR T cell in vivo antitumor response and predict clinical outcome

Having established that DNMT3A KO improves antitumor activity in solid tumor models, we next sought to corroborate these findings in the most successful CAR T cell product to date, CD19-CAR T cells. We generated DNMT3A KO CAR T cells expressing a CD19-CAR with the same structure (including antigen binding and signaling domains; fig. S27) used in several previously published clinical studies (2, 3, 38, 39). As expected, the DNMT3A-edited CD19-CAR T cells exhibited improved antitumor activity and survival in a CD19- positive leukemia xenograft model (Fig. 6, A to D). To determine whether mice treated with DNMT3A KO CAR T cells had established functional memory, the two complete responders were rechallenged with an additional dose of BV173 at day 113 (fig. S28A), which they successfully rejected (fig. S28, B and C). To ensure that the rejection was fully dependent on CD19-CAR–mediated cytotoxicity, we then injected the animals with BV173.CD19 KO cells (fig. S28A), which were successfully implanted (fig. S28, D and E).

Next, to gain insight into whether our epigenetically regulated multipotency program predicts the outcome of CAR T cell therapy, we took advantage of a publicly available RNA sequencing expression dataset of 34 CD19-CAR T cell products that were infused into patients with CLL (3). Patients with CLL on the clinical study could be divided into four groups according to their clinical response and median peak expansion (MPE) of CAR T cells: 21 nonresponders (NRs; MPE: 205), 4 partial responders (PRs; MPE: 13,257), 5 complete responders (CRs; MPE: 58,570), and 3 PRs followed by relapse with transformed B cell lymphoma (PR_{TD}; MPE: 130,258). On the basis of our analysis, the generated preinfusion CAR T cell product of responders (CR, PR, or PR_{TD}) had significantly higher expression of DNMT3A-targeted genes compared to those of nonresponders (NR versus CR: $P < 0.01$; PR: $P < 0.01$; and PR_{TD}: $P < 0.05$; Fig. 6E; individual DNMT3A-targeted genes are shown in fig. S29). Because responder CAR T cells also had a 65- to 635-fold greater expansion after infusion relative to nonresponder CAR T cells, these data, similar to our preclinical studies, highlight that the expansion potential of T cells is closely linked to expression of DNMT3A-targeted genes.

We next used the list of differentially expressed genes (DEGs) between DNMT3A KO and Ctrl CAR T cells obtained from our in vitro stimulation experiments (Fig. 3A) to determine whether transcripts, directly or indirectly regulated by DNMT3A, could predict clinical responders or peak expansion. On their own, the transcriptional programs indirectly affected by DNMT3A deletion were not predictive (fig. S30A). We then used the DNMT3A DMR list to filter out DEGs that were indirectly linked to DNMT3A programming (genes that do not have DNMT3A-associated changes in DNA methylation programming but are differentially expressed between Ctrl and DNMT3A KO CAR T cells). The gene expression profile that focused on genes that contain DMRs was able to differentiate between responders and nonresponders and peak expansion (fig. S30B). Thus, as in our preclinical models, DNMT3A-regulated genes play a critical role in determining the antitumor potential of human CAR T cells.

DISCUSSION

Collectively, our studies demonstrate that genetic disruption of DNMT3A in CAR T cells prevents methylation of several key genes regulating human T cell differentiation. The resulting stem-like CAR T cells maintain their antigen-dependent proliferative capacity and effector functions during prolonged stimulation both in vitro and in vivo where they exhibit superior tumor control. Broadly, our results have identified a mechanism in which DNMT3A-mediated methylation of the *TCF7* and *LEF1* loci, as well as other transcriptional regulators, serves to stably limit T cell developmental potential under conditions of persistent antigen exposure. These findings are consistent with previous reports that show that calibrating T cell activation to maintain expression of naïve and memory-associated genes and suppress T cell differentiation yields a durable antitumor response with maintenance of effector functions in CAR T cells (40). Additional studies have shown that $CD4^+$ and $CD8^+$ CAR T cells derived from naïve, stem cell memory, and central memory subsets were more effective in clearing tumors than those from the effector memory subset (41–43). Prior studies documenting a correlation between antitumor activity and peak proliferation of $CD4^+$ and $CD8^+$ CAR T cells have served as the basis for identifying determinants of CAR T cell peak expansion (44). Thus, our data further support a rationale for epigenetic-based approaches to extend the survival and effector response of CAR T cells.

Our whole-genome DNA methylation profiles suggest that DNMT3A KO CAR T cell's retained survival and effector capacity are coupled to maintenance of preexisting epigenetically permissive programs at stemness-associated loci, including *TCF7*, *LEF1*, and *CCR7*. These data are consistent with recently published results indicating that the presence of the transcription factor TCF7 in $CD8^+$ T cells is predictive of positive clinical outcomes in patients treated with immune checkpoint therapy (15). Moreover, transcriptional profiling analyses of the $CD8^+$ T cells from the patients treated in these studies revealed two major T cell states. One $CD8^+$ T cell subset associated with increased expression of genes linked to memory, activation, and cell survival was enriched in responders to immune checkpoint blockade. Conversely, the other subset exhibited genes linked to exhaustion and was associated with nonresponders (43, 45). In addition, a recent case report has highlighted the role of epigenetic reprograming in determining T cell fate (46). The patient received a CAR T cell product in which a single CAR T cell had one disrupted tet methylcytosine dioxygenase 2 (TET2) allele, an enzyme that regulates DNA demethylation, due to lentiviral integration, and a hypomorphic mutation in the second TET2 allele. This resulted in selective CAR T cell expansion, which induced CLL remission (46). CAR T cell dysfunction can also be overcome with other approaches. For example, one study assessing the role of the activator protein 1 (AP-1) transcriptional network in CAR T cells demonstrated that sustained expression of cellular JUN (cJUN) in CAR T cells can enhance their proliferative functions and antitumor activity (47). Additional studies are needed to further define transcriptional networks and epigenetic programs that reinforce the functional state of T cells. In addition, longitudinal epigenetic and transcriptional analysis of CAR T cells infused into xenograft models is warranted. These published results, together with our

new findings, demonstrate the importance of preserving a stem-like differentiation state of human T cells in establishing effective cellular therapies.

Although our results focus on CAR T cells, this approach can be broadly applied to the field of T cell therapy. Given that TCR-driven suppression of effector and memory potential are hallmarks of T cell exhaustion, we leveraged our past analyses of bona fide exhausted mouse $CD8^+$ T cells from the lymphocytic choriomeningitis virus (LCMV) model system (48, 49) to provide a molecular definition for human T cell exhaustion. Our data have identified the downstream T cell stemness (TCF7 and LEF1) pathways as targets for epigenetic silencing during the progressive development of T cell exhaustion. Recent efforts to identify the population of T cells that contribute to therapeutic efficacy in models of immunotherapy have similarly identified $CD28^+$ T cells as the primary source for antitumor responses (50, 51). These results, together with our data presented here, as well as studies reporting a critical role for IL-10 in suppressing T cell effector responses (52), suggest that the increase in IL-10 signaling that we observe in exhaustion-resistant DNMT3A KO CAR T cells serves to limit the cells from becoming overstimulated. These data highlight DNMT3A as a central mediator of T cell exhaustion and suggest that this epigenetic process may serve as a universal mechanism to restrict mammalian T cell fate potential.

An increase in IL-10 production was observed in DNMT3A KO CAR T cells, and knocking out IL-10 in DNMT3A KO CAR T cells abrogated their proliferative advantage over Ctrl CAR T cells. IL-10 has been previously shown to stimulate the proliferation of activated $CD8^+$ T cells and augment the survival and function of memory-type T cell effectors (53). The up-regulated secretion of IL-10 in DNMT3A KO CAR T cells appears to be coupled to the retained proliferative capacity of the DNMT3A KO $CD8^+$ T cells and may suggest that epigenetic reprogramming of the cells selectively enriches for the survival of a memory population. Recent studies have reported that IL-10 increases the antitumor activity of transgenic TCR T cells by metabolically reprogramming the T cells to increase oxidative phosphorylation (54), suggesting that further studies evaluating metabolic changes incurred by deletion of DNMT3A in CAR T cells are warranted. Although the precise mechanism requires further investigation, our study clearly demonstrates that there is a link between IL-10 signaling and epigenetically regulated CAR T cell expansion in the context of chronic antigen stimulation.

We tested the effect of DNMT3A KO in T cells expressing CARs with ζ, CD28ζ, 41BBζ, CD27ζ, or OX40ζ endodomains targeting tumor-associated antigens expressed on solid tumors (HER2, EphA2, and IL13Rα2). For all CAR T cell populations, we observed improved antigen-dependent T cell expansion and sustained cytolytic activity, highlighting the universal role of DNMT3A-dependent epigenetic programs in restricting the developmental potential of CAR T cells. In vivo, DNMT3A KO CAR T cells efficiently eradicated tumors, resulting in an overall survival advantage compared to controls in three of four animal models. Of interest, in the only model in which the overall survival advantage was not improved, we observed, as previously reported (25), antigen loss variants, highlighting that, in addition to increasing expansion and persistence, targeting of multiple antigen will be necessary to prevent immune escape.

Although DNMT3A mutations have been previously associated with myelodysplastic syndromes and leukemia (55–57), note that these occur in hematopoietic progenitor cells or lineage precursors. For example, the pathologic phenotype of DNMT3A-mutated T cell–derived leukemias is usually consistent with an early T cell precursor–derived lesion (57). This is confirmed in murine models, where cooperative KO of DNMT3A with activating mutations of *Notch1* in hematopoietic cells and early progenitors accelerates leukemogenesis, but, in mature T cells, is not sufficient to promote leukemogenesis (57). Likewise, we have shown that the retained proliferative capacity of DNMT3A KO CAR T cells reported here is strictly antigen dependent. In addition, our prior analysis of murine $CD8^+$ T cells responding to an acute viral infection demonstrates that deletion of DNMT3A after T cell activation does not impair the cell's ability to undergo contraction after viral control. Furthermore, there was no evidence of T cell or natural killer cell lymphoma or leukemia in these murine T cell studies (57, 58). Thus, preservation of DNMT3A KO CAR T cells' proliferative capacity occurs without resulting in uncontrolled cellular division. Last, a report of one individual with somatic mosaicism for $DNMT3A^{R771Q}$ mutation revealed a long- term enrichment of *DNMT3A* mutant cells in hematopoietic lineages without accelerated mutagenesis or development of malignancy (59).

Potential limitations of our study include (i) the fact that we used exogenous IL-15 in our in vitro studies, (ii) potential for alloreactivity, and (iii) limited testing of DNMT3A KO in Food and Drug Administration (FDA)–approved CAR T cell products. Although we did perform our in vitro repeat stimulation assays in the presence of IL-15, we did not administer IL-15 to mice. In repeat stimulation assays without IL-15, DNMT3A KO CAR T cells still had a proliferative advantage and produced more IL-10 in comparison to Ctrl KO CAR T cells; however, the effect was less pronounced. We and others have observed differential in vitro and in vivo requirements for exogenous cytokines of CAR T cells with second genetic modifications (47, 60), highlighting differences between in vitro culture systems and preclinical in vivo models, which more closely mimic human tumors. Alloreactivity through endogenous TCRs is a concern when second genetic modifications are introduced into CAR T cells (61). However, our in vitro studies revealed no evidence of increased alloreactivity of DNMT3A KO CAR or NT T cells in comparison to their unmodified counterparts. Likewise, DNMT3A KO CAR T cells did not induce xenogeneic graft versus host disease and, in rechallenge experiments, only rejected antigen-positive tumor cells. Last, we only evaluated DNMT3A KO in one of the currently FDA-approved CAR T cell products (CD19.41BB.ζ CAR T cells). Future studies should focus on extending our findings to other CAR T cell products, which are currently used in the clinic, including CD19.CD28ζ-CAR T cells.

In conclusion, we have shown that human CAR T cell exhaustion is coupled to de novo DNA methylation of genes that regulate T cell multipotency. Results from our study further highlight the relationship between DNA methylation programs, T cell differentiation, and clinical outcomes. Although our study documents the feasibility of exploiting epigenetic programs to improve current CAR T cell therapy approaches and develop combinatorial therapies, the identified DNMT3A exhaustion signature might also be useful as a biomarker to select patients and predict responses.

MATERIALS AND METHODS

Study design

The objective of this study was to define the functional effects of DNMT3A KO in CAR T cells. For all experiments, the number of replicates, statistical test used, and *P* values are reported in the figure legends. The reported replicates refer to biological replicates (T cells from different healthy donors). All in vitro experiments in the main text were performed at least three times, and no outliers or other data points were excluded. For in vivo experiments, NSG mice were treated with CAR T cells from one to two different healthy donors. Cages of mice were randomly assigned to treatment groups. The technicians injecting and imaging the mice were not blinded to the names of treatment groups, but they were unaware of their meaning or expected results. The bioluminescence-defined end point (total flux greater than 1×10^{10} photons/s) was selected to maximize animal welfare as larger tumor burdens were associated with clinical signs of pain and distress.

Cell lines

U373 glioma and 293T (human embryonic kidney) cells were purchased from the American Type Culture Collection (ATCC). LM7 osteosarcoma cells were provided by E. Kleinerman (MD Anderson Cancer Center) in 2011. U373 cells were maintained in RPMI 1640 supplemented with 10% fetal bovine serum (FBS) and 2 mM GlutaMAX. LM7 and 293T were maintained in Dulbecco's modified Eagle's medium with the same supplements. The production of U373 and LM7 cells expressing enhanced green fluorescent protein (GFP) and firefly luciferase (eGFP.ffLuc) has been previously described (26, 62). BV173 (B cell precursor ALL) cells were obtained from the German Collection of Microorganisms and Cell Cultures and maintained in RPMI 1640 with 10% FBS and 2 mM GlutaMAX. BV173 cells were modified to express a previously described yellow fluorescent protein (YFP) and firefly luciferase (YFP.ffLuc) vector (vCL20SF2-Luc2a-YFP) (63) using lentiviral transduction. The production of BV173 with CD19 KO has been previously described (64).Cell lines were routinely validated using the ATCC short tandem repeat (STR) Profiling Cell Authentication Service and tested for mycoplasma on a regular basis.

Production of viral vectors

The generation of retroviral vectors encoding the EphA2-CAR with a 41BBζ endodomain as well as HER2-, IL13Rα2-, or EphA2-CARs with a CD28 transmembrane domain and CD28ζ signaling domain or IL-15 has been previously described (27–29). The retroviral vector encoding the first-generation HER2.ζ-CAR was created by subcloning the HER2-specific single-chain variable fragment (scFv), FRP5 (27, 65), into a retroviral vector encoding an expression cassette with a CD28 transmembrane and ζ signaling domain (66). The retroviral vectors encoding the second-generation EphA2 CD27ζ and OX40ζ endodmains were cloned with In-Fusion cloning, using the EphA2.CD28ζ-CAR as a vector and our previously published CD70 and IL13Rα2-CARs as the template for polymerase chain reaction (PCR) of the CD27 and OX40 costimulatory domains, respectively (28, 67). To create transgenic DNMT3A, DNMT3A open reading frame (NM_175629.2, GenScript) was cloned into a retroviral pSFG vector downstream of CD20 and a 2A sequence with a FLAG-tag added to the C terminus using NEBuilder [New England Biolabs (NEB)].

To make the sequence resistant to cleavage by Cas9, two silent mutations, one in the sgRNA recognition sequence and one in the PAM, were incorporated using the QuikChange lightning mutagenesis kit (Agilent Technologies). RD114-pseudotyped retroviral particles were generated as previously described (62) by transient transfection of 293T cells using GeneJuice Transfection Reagent (EMD Millipore). Viral supernatants were collected 48 hours after transfection for the same-day T cell transduction, or snap-frozen, and stored at −80°C until use. The self-inactivating third-generation lentivirus vector that encodes a CD19-specific CAR with signaling domains of 41BB and CD3ζ driven by an MND promoter has been described previously (68, 69) and was produced by transient transfection of 293T cells followed by vector particle purification by anion- exchange chromatography (70).

Generation of DNMT3A KO CAR T cells

This study was conducted with approval from the St. Jude Children's Research Hospital Institutional Review Board (IRB). Peripheral blood mononuclear cells (PBMCs) were isolated from consented healthy donors (IRB XPD15–086) by density gradient separation using Lymphoprep (STEMCELL Technologies, Vancouver, BC). Cells were then plated in 24-well non–tissue culture–treated plates precoated with 250 ng each of anti-CD3 and anti-CD28 monoclonal antibodies (Miltenyi Biotec). Culture medium for initial stimulation was RPMI 1640 supplemented with 10% FBS and 2 mM GlutaMAX (Thermo Fisher Scientific). IL-7 and IL-15 (PeproTech) were added at 10 and 5 ng/ml, respectively, 24 hours later. The following day, cells were electroporated with *Streptococcus pyogenes* Cas9-sgRNA RNP complexes targeting DNMT3A, IL-10, or mCherry (Ctrl) 24 hours later by transduction on RetroNectin-coated plates (Takara Bio). RNPs were precomplexed at an sgRNA:Cas9 ratio of 4.5:1, prepared by adding 3 μl of 60 μM sgRNA (Synthego) to 1 μl of 40 μM Cas9 (MacroLab, University of California, Berkeley) and frozen for later use. For single-gene KO, 6×10^5 T cells were resuspended in 20 μl of R buffer and added to 4 μl of RNP. For double-gene KO, 6×10^5 T cells were resuspended in 16 μl of R buffer and added to 4 μl of RNP1 (DNMT3A) and 4 μl of RNP2 (IL-10). Ten microliters of cells + RNP was electroporated with three pulses of 10 ms at 1600 V using the Neon Transfection System (Thermo Fisher Scientific). Two 10-μl electroporation reactions were pooled in one well of a 48-well tissue culture-treated plate containing RPMI 1640 supplemented with 20% FBS, GlutaMAX, IL-7 (10 ng/ml), and IL-15 (5 ng/ml) for 72 hours. After recovery, the medium was switched to RPMI 1640 containing 10% FBS and GlutaMAX. The cells were then expanded for 10 to 12 days with IL-7 and IL-15 added every 2 to 3 days at the same concentrations indicated above.

For CAR T cells expressing transgenic DNMT3A (tD), cells were prepared mostly as described previously. The lone modification was that T cells were electroporated in the morning and transduced with the vector encoding tD in the afternoon. T cells were transduced again the following morning with the vector encoding the HER2.ζ-CAR.

$CD4^+$ and $CD8^+$ T cells were purified using CliniMACS Plus instrument and reagents (Miltenyi Biotec) and were cultured in X-VIVO 15 medium (Lonza) containing 5% Human AB serum (Valley Biomedical) and 10 ng/ml each of recombinant human IL-7 and IL-15

(Miltenyi Biotec) (referred to as expansion medium) and activated with 1:87.5 (v/v) of T Cell TransAct reagent (Miltenyi Biotec) for 18 to 24 hours in T75 flasks. On day 1, activated T cells were transduced with CD19-CAR lentiviral vector at a multiplicity of infection of 25 in the presence of protamine sulfate (4 μg/ml) for 18 to 24 hours. On day 2, cells were washed with MaxCyte Electroporation Buffer (GE Healthcare Life Science), mixed with precomplexed RNP at 4 μM, and electroporated with the MaxCyte ATX Electroporation System using T cell program 1. After electroporation, cells were transferred to prewarmed expansion medium and incubated at 37°C for 1 hour before being transferred to a G-Rex-6M culture plate (Wilson Wolf) for expansion. On day 5, IL-7 (10 ng/ml) and IL-15 (10 ng/ml) were added again into the medium. On day 7 or 8, expanded gene-edited CAR T cells were harvested, washed with Plasma-Lyte A containing 4% human serum albumin (HSA), and cryopreserved in Plasma-Lyte A containing 6% pentastarch, 5.75% HSA, and 5% dimethyl sulfoxide (DMSO) using a controlled-rate freezer. Cells were thawed and cultured in the expansion medium for 2 days, washed, and resuspended in phosphate-buffered saline (PBS) for tail vein injection into NSG mice.

Guide RNA design and validation

All guide RNAs were designed and validated by the Center for Advanced Genome Engineering at St. Jude Children's Research Hospital. sgRNAs were designed to target unique sites within the genome with at least 3 base pairs (bp) of mismatch between the target site and any other site in the genome whenever possible, and common single-nucleotide polymorphisms were avoided. To disrupt DNMT3A function, we designed sgRNAs targeting the DNMT3A catalytic domain located in exon 19 (g2; figs. S1B and S8) (24). To mitigate the risk of any off-target–mediated functional effects, we used additional sgRNAs (guides 1, 3, and 7; fig. S8). Guide 3 was previously validated and published (24). As an additional control, sgRNAs were designed to a sequence in mCherry that does not occur in the human genome with up to 3 bp of mismatch. To assess initial guide RNA activity, mCherry, *DNMT3A*, or *IL10* sgRNAs were nucleofected as RNPs (100 μM sgRNA and 50 μM Cas9 protein using solution P3 and program FF-120) into K562; genomic DNA from transfected cells was harvested 3 days after nucleofection; and nonhomologous end joining rates were determined using targeted next-generation sequencing (NGS) followed by analysis with CRIS.py (71). sgRNAs were then transfected into T cells as described in the previous section, and Western blots were used to further validate activity (loss of protein) or NGS. Protospacer sequences and primer sequences for NGS are provided in table S1.

Western blot analysis

KO efficiency was determined by Western blot. Ctrl and DNMT3A KO CAR T cells were washed with PBS and lysed with radioimmunoprecipitation assay buffer (Cell Signaling Technologies) with Halt Protease and Phosphatase Inhibitor Cocktail (Thermo Fisher Scientific) the day of their first use in experiments. Protein quantification was performed using a bicinchoninic acid protein assay (Thermo Fisher Scientific), and 30 μg of total protein was loaded on a polyacrylamide gel and then transferred to nitrocellulose membranes (Bio-Rad). Membranes were blocked with 5% milk in tris-buffered saline + 0.1% Tween 20 (Sigma-Aldrich) for 1 hour at room temperature. The membranes were then probed with a monoclonal rabbit anti-human DNMT3A antibody (clone

D23G1, Cell Signaling Technologies) or a monoclonal mouse anti-human glyceraldehyde phosphate dehydrogenase (GAPDH) antibody (clone 0411, Santa Cruz Biotechnologies) overnight at 4°C. Membranes were then washed and probed with a secondary anti-rabbit immunoglobulin G (IgG)–horseradish peroxidase (HRP) (Jackson ImmunoResearch) or anti-mouse IgG-HRP (sc-2005, Santa Cruz Biotechnology) for 1 hour at room temperature. Protein expression was visualized using Femto Enhanced Chemiluminescent Substrate (Thermo Fisher Scientific), and images were acquired and analyzed using a LI-COR Odyssey instrument and software (LI-COR Biosciences).

Mouse tumor xenograft models

NSG mice were obtained from breeding colonies maintained by the St. Jude Animal Resource Center. All animal experiments were performed on protocols approved by the St. Jude Institutional Animal Care and Use Committee. Eight- to 10-week-old male and female mice were used in both the glioma and osteosarcoma models. For the local LM7 model, 1×10^6 LM7.eGFP.ffLuc cells were injected intraperitoneally on day 0. EphA2.CD28ζ-CAR T cells (1×10^5) were injected intraperitoneally on day 7. For the disseminated LM7 model, mice were injected intravenously with 2×10^6 LM7.eGFP.ffLuc cells and, on day 28, with 1×10^6 HER2.ζ-CAR T cells. The orthotopic U373 glioma model has been described previously (28). Briefly, 5×10^4 U373.eGFP.ffLuc cells were injected through a burr hole 1 mm anterior and 2 mm to the right of the bregma at a depth of 3 mm. IL13Rα2.CD28ζ-CAR/IL-15 T cells (2×10^6) were injected 7 days later in the same location. For the BV173 B-Cell acute lymphoblastic leukemia (B-ALL) xenograft model (72), 3×10^6 BV173.eGFP.ffLuc cells were injected intravenously on day 0. CD19.41BBζCAR T cells (2×10^6) were injected intravenously on day 7. The rechallenge experiment with BV173 cells is described in detail in fig. S28A. For each model, CAR T cells were generated from a different healthy donor. Tumor burden was assessed weekly using bioluminescent in vivo imaging system (IVIS). Quantification of tumor burden was performed using Living Image software (PerkinElmer). A region of interest (head for U373 and total body for LM7) was drawn around each mouse, and total flux was recorded in units of photons per second.

Isolation of T cells for WGBS

NSG mice were injected intraperitoneally with 1×10^6 LM7 tumor cells on day 0. On day 7, mice were injected with 1×10^5 EphA2.CD28ζ-CAR T cells. On day 14, an intraperitoneal wash was performed to isolate T cells for WGBS. Briefly, each mouse was injected with 3 to 5 ml of PBS into the peritoneal cavity, the belly was gently massaged, and the PBS was withdrawn with a syringe. For the five mice receiving the same treatment (Ctrl or DNMT3A KO CAR T cells), the contents of each peritoneal wash were pooled before being spun down and FACS-purified.

Repeated stimulation assay

Ctrl and DNMT3A KO CAR T cells were cocultured with U373 or LM7 cells at an E:T ratio of 2:1 in the presence of IL-15 (5 ng/ml). Seven days later, T cells were counted and replated with fresh tumor cells at the same 2:1 ratio in the presence of IL-15 (5 ng/ml). The T cells continued to be counted and stimulated with fresh tumor cells on a weekly basis until the T

cells stopped killing tumor cells. Cocultures with Ctrl, DNMT3A KO, IL-10 KO, and DKO CAR T cells were also performed in the presence or absence of IL-10 (5 ng/ml; PeproTech).

Measurement of cytokine production

At each stimulation of the repeated stimulation assay, culture supernatant was collected 24 hours after plating T cells with tumor cells for analysis of cytokine production. Cytokine production was assessed by a 14-plex human cytokine quantification kit (Millipore Sigma). Analysis was performed using a Luminex FLEXMAP 3D instrument and software (Luminex Corporation). An IL-10 ELISA (PeproTech) was used to confirm successful KO of IL-10.

Cytotoxicity assays

A CellTiter96 AQueous One Solution Cell Proliferation Assay (Promega) was used to assess CAR T cell cytotoxicity as previously described (26). Briefly, tumor cells were incubated with varying amounts of CAR T cells to assess cytotoxicity at a range of E:T ratios. Twenty-four hours later, the medium and T cells were removed, and the remaining tumor cells were quantified with the CellTiter96 AQueous One Solution Reagent containing a tetrazolium compound [3-(4,5-dimethylthiazol-2-yl)-5-(3-carboxymethoxyphenyl)-2-(4-sulfophenyl)-2*H*-tetrazolium, inner salt (MTS)] and an electron coupling reagent [phenazine ethosulfate (PES)]. Medium only and tumor only served as controls to assess percent cytotoxicity. Cytotoxicity assays were performed using unstimulated CAR T cells (first stimulation) and CAR T cells that had previously been exposed to tumor cells three times (fourth stimulation).

CAR T cell antigen dependence assay

Survival of serially stimulated DNMT3A KO CAR T cells in the absence of tumor was assessed by the positive selection of $CD3^+$ coculture cells (Miltenyi Biotec) followed by a 7-day culture in the absence of tumor cells with or without IL-15. Live and dead cells were enumerated by flow cytometry. Samples were washed with PBS, stained with a 1:1000 dilution of viability dye LDA (Invitrogen) or eFluor 520 (Invitrogen), washed with PBS, and resuspended in 1× annexin V staining buffer (BD Biosciences) with 5 μl of annexin V phycoerythrin (PE) or annexin V allophycocyanin (APC) (BD Biosciences). Data were acquired on a BD FACSCanto and analyzed using FlowJo version 10.5.3.

Immunophenotyping by flow cytometry

Samples were phenotyped before and after coculture with tumor cells. All surface antibody and viability dye staining was performed in PBS + 1% FBS at 4°C for 30 min. Intracellular staining was performed using the eBioscience Foxp3/Transcription Factor Staining Buffer Set (Invitrogen). For these samples, after staining with surface antibodies and viability dye as described above, cells were washed with PBS + 1% FBS, fixed/permeabilized for 1 hour at 4°C, washed with permeabilization buffer twice, stained with intracellular antibodies at room temperature for 30 min, and again washed with permeabilization buffer twice before being resuspended in PBS + 1% FBS. For live cell discrimination, samples were stained with a 1:1000 dilution of one of the following viability dyes: Fixable Viability Dye eFluor 506 (Invitrogen), Fixable Viability Dye eFluor 520 (Invitrogen), Fixable Viability Dye

eFluor 780 (Invitrogen), LDA (Invitrogen), or Ghost Dye Violet 510 (Tonbo Biosciences). The following antibodies were used in phenotypic analysis: CD3 Brilliant Violet (BV) 605 (BD Biosciences, clone SP34–2; 2.5 μl per test), CD3 BV421 (BD Biosciences, clone SK7; 2.5 μl per test), CD4 PE-Cy7 (BD Biosciences, clone SK3; 2.5 μl per test), CD4 APC-Cy7 (BD Biosciences, clone SK3; 2.5 μl per test), CD8 Peridinin chlorophyll protein complex (PerCP)-Cy5.5 (BD Biosciences, clone HIB22; 2.5 μl per test), CD8 AF488 (BioLegend, clone HIT8a; 2.5 μl per test), CD8 BV785 (BioLegend, clone RPA-T8; 2.5 μl per test), CD28 PE (BD Biosciences, clone CD28.2; 5 μl per test), CD45RO APC-Cy7 (BioLegend, clone UCHL1; 2.5 μl per test), CCR7 Alexa Fluor (AF) 488 (BioLegend, clone G043H7; 2.5 μl per test), Tim3 PE-Cy7 (BioLegend, clone F38–2EZ; 2.5 μl per test), TCF7 AF488 (Cell Signaling Technologies, clone C63D9; 1 μl per test), LEF1 AF647 (Cell Signaling Technologies, clone C12A5; 1 μl per test), and Ki67 BV510 (BD Biosciences, clone B56; 2.5 μl per test). Isotype-matched controls were run for each experiment. Samples were acquired on a BD FACSLyric, BD FACSCanto, or BD LSRFortessa, and list mode files were analyzed using FlowJo version 10.5.3 (BD Biosciences).

FACS sorting for WGBS

WGBS was performed on CAR T cells that were taken directly from culture or had been previously stimulated with fresh U373 tumor cells four times, with the stimulations separated by 1 week or 1 day, as indicated in the text. WGBS was also performed on T cells extracted from intraperitoneal LM7-bearing mice by intraperitoneal wash 7 days after T cell injection. Ctrl KO, DNMT3A KO, and, for some conditions, IL-10 KO and DKO CAR T cells were FACS-purified on the basis of live $CD8^+$ phenotyping using a BD FACSAria II (BD Biosciences). DNA was extracted, and bisulfite was converted using a Zymo EZ DNA methylation-direct kit per the manufacturer's instructions. This converted all unmethylated cytosines to uracils and protected the methylated cytosines from deamination. Bisulfite-modified DNA libraries were sequenced using Illumina HiSeq, and sequencing data were mapped to the HG19 human genome. Differences in CpG methylation across the genome were visualized using the Integrated Genome Viewer software (73) and quantified using a Bayesian hierarchical model to detect regional methylation differences with at least three CpG sites (74).

T cell subset isolation

For experiments using purified cell populations, PBMCs from fresh blood from healthy consented donors were isolated by centrifugation in BD Vacutainer CPT tubes (BD Biosciences) and enriched before sorting. After $CD8^+$ T cell enrichment, naïve and memory $CD8^+$ T cell compartments were FACS-purified. Cells were stained in sterile PBS containing 4% FBS with the same antibodies described above. Individual cell populations were sorted using a BD FACSAria II (BD Biosciences). Naïve $CD8^+$ T cells were defined as live $CD8^+$, $CCR7^+$, and $CD45RO^-$ cells. The memory $CD8^+$ T cell compartment was sorted on the basis of live $CD8^+$, $CD45RO^+$ expression. The memory compartment included Tem ($CCR7^-$) and Tcm ($CCR7^+$) $CD8^+$ T cells. Sorted cells were checked for purity and determined to be at least 95% of the desired phenotype.

Transduction efficiency evaluation

Efficiency of retroviral transduction was determined by flow cytometry. All staining and washing was performed with PBS + 1% FBS. For the IL13Rα2-CAR and CD19-CAR, T cells were washed, incubated with 7 μl of recombinant IL13Rα2-F_c fusion protein (R&D Systems) or 3 μl of recombinant human CD19-F_c fusion protein (R&D Systems) at room temperature for 1 hour, washed, and stained with 1 μl of anti-human IgG F_c PE (SouthernBiotech) for 30 min at 4°C. All other transgene staining was performed at 4°C for 30 min with the following antibodies: HER2-CAR: anti-mouse Fab AF647 (Jackson ImmunoResearch; 2 μl per test); EphA2-CAR: anti-human CD19 PE (Beckman Coulter; 3 μl per test) or anti-human Fab AF647 (Jackson ImmunoResearch; 2 μl per test); and IL-15 vector: anti-human nerve growth factor receptor (NGFR) BV421 (BD Biosciences; 5 μl per test). Samples were acquired on a BD FACSLyric or BD FACSCanto, and list mode files were analyzed using FlowJo version 10.5.3 (BD Biosciences).

Bisulfite sequencing methylation profiling and data analysis

Genomic DNA was isolated from FACS-purified T cells and processed as previously described (21). Briefly, DNA was extracted from the sorted cells using a DNA extraction kit (QIAGEN) and then bisulfite-treated using an EZ DNA methylation kit (Zymo Research) or an EZ DNA methylation-direct kit (Zymo Research). The bisulfite-modified DNA sequencing library was generated using the EpiGnome kit (Epicentre) per the manufacturer's instructions and then sequenced using an Illumina HiSeq or NovaSeq instrument. Sequencing data were aligned to the hg19 genome using BSMAP2.74 (75). DMRs were identified using Bioconductor package dispersion shrinkage for sequencing (DSS) (76). We first performed a statistical test of differentially methylated locus (DML) using the DMLtest function (smoothing = TRUE) in DSS; the results were then used to detect DMRs using the CallDMR function in DSS, and the *P* value threshold for calling DMR was 0.01. The minimum length for defining a DMR was set to 50 bp, and the minimum number of CpG sites for defining a DMR was 3. The methylation plots are a visualization of the DMRs (using ≤30 or >30% differences in methylation) in genes predetermined to be statistically significant. The GSEA analyses were performed using 108 DNMT3A-target transcription factors as gene signature on gene expression data from GSE23321 (77). IPA was performed using DNMT3A-targeted genes. Enrichr was used for GO analysis.

We previously established a human $CD8^+$ T cell DNA methylation–based MPR using a machine learning approach (78). Briefly, to identify the methylation state of CpG sites associated with the T cell multipotent potential, a supervised analysis was performed between the methylomes from two naïve and four HIV-specific $CD8^+$ T cells [methylation difference ≥ 0.4 and false discovery rate (FDR) ≤ 0.01]. This analysis results in identification of 245 CpG sites that were hypomethylated in naïve $CD8^+$ T cells compared to HIV-specific $CD8^+$ T cells. This set of the CpGs was then used as an input to the one-class logistic regression to calculate the multipotency signature using only the HIV-specific and naïve $CD8^+$ T cells (training datasets) (79, 80). Once the signature was obtained, it was then applied to the naïve $CD8^+$ T cells, Tscm, and Tem from healthy donors, and CAR T cell methylomes (test datasets). The

score was calculated as the dot product between the DNA methylation value and the signature. The score was subsequently converted to the [0, 1] range. Datasets with multipotency indices closer to 1 were more similar to naïve cells. In addition, data were analyzed through the use of IPA (QIAGEN Inc.; https://apps.ingenuity.com/ingsso/login?service=https%3A%2F%2Fanalysis.ingenuity.com%2Fpa%2Flogin%2Fcas).

CHANGE-seq

Genomic DNA from T cells was isolated using the Gentra Puregene Kit (QIAGEN) according to the manufacturer's instructions. Purified genomic DNA was tagmented with a custom Tn5 transposome to an average length of 400 bp, followed by gap repair with KAPA HiFi HotStart Uracil+ DNA Polymerase (KAPA Biosystems) and Taq DNA ligase (NEB). Gap-repaired tagmented DNA was treated with USER enzyme (NEB) and T4 polynucleotide kinase (NEB). Intramolecular circularization of the DNA was performed with T4 DNA ligase (NEB), and residual linear DNA was degraded by a cocktail of exonucleases containing Plasmid-Safe ATP-dependent DNase (Lucigen), Lambda exonuclease (NEB), and exonuclease I (NEB). In vitro cleavage reactions were performed with 125 ng of exonuclease-treated circularized DNA, 90 nM SpCas9 protein (NEB), Cas9 nuclease buffer (NEB), and 270 nM sgRNA in a 50-μl volume. Cleaved products were A-tailed, ligated with a hairpin adaptor (NEB), treated with USER enzyme (NEB), and amplified by PCR with barcoded universal primers NEBNext Multiplex Oligos for Illumina (NEB), using KAPA HiFi Polymerase (KAPA Biosystems). Libraries were quantified by quantitative PCR (KAPA Biosystems) and sequenced with 150-bp paired-end reads on an Illumina NextSeq instrument. Circularization for high-throughput analysis of nuclease genome-wide effects by sequencing (CHANGE-seq) data analyses were performed using open-source circularization for in vitro reporting of cleavage effects by sequencing (CIRCLE-seq) analysis software (https://github.com/tsailabSJ/circleseq).

Histology and immunohistochemistry

Formalin-fixed tissues were decalcified in formic acid and were processed and embedded in paraffin by standard techniques, sectioned at 4 μm, mounted on positively charged glass slides (Superfrost Plus, Thermo Fisher Scientific), and dried at 60°C for 20 min. Tissue sections were then stained with hematoxylin and eosin or subjected to immunohistochemical staining for $CD3^+$ T cells using a rabbit polyclonal antibody raised against CD3 (1:1000; catalog no. sc1127, Cell Signaling Technologies). Tissue sections underwent antigen retrieval in prediluted Cell Conditioning Solution (CC1; catalog no. 950–124; Ventana Medical Systems) for 32 min on a Discovery Ultra immunostainer (Ventana Medical Systems). Binding of primary antibodies was detected using OmniMap anti-rabbit (#760–4311, Ventana Medical Systems), with the DISCOVERY ChromoMap DAB Kit (Ventana Medical Systems) as chromogenic substrate. Stained sections were examined by a pathologist blinded to the experimental group assignments.

To quantify $CD3^+$ cells in brain tumors, whole-section imaging of sections was completed using a NanoZoomer S210 digital slide scanner (Hamamatsu). Scanned tissue sections, with CD3-positive cells labeled using 3,3′-diaminobenzidine (DAB) immunohistochemistry, were analyzed using the Indica Labs HALO image analysis platform. A pathologist

manually annotated tumor outlines on each slide and used Indica Labs analysis modules CytoNuclear v2.0.5 to detect DAB-positive and DAB-negative cells within tumors. The total tumor area and numbers of CD3-positive and CD3-negative cells within tumors were automatically detected and counted using the Indica Labs CytoNuclear v2.0.9 analysis module.

DNMT3A gene expression score

Transcript counts were obtained from Fraietta *et al.* (46) "table S5B: Transcriptomic profiling of CAR-stimulated CTL019 infusion products" and then filtered, normalized, and analyzed using the R packages "edgeR" (81) and "limma" (82). PCA was conducted on the entirety of the expression data, revealing a single partial responder data point that was an obvious outlier in comparison to the other samples (and therefore excluded from downstream analyses). One thousand thirty-three gene identifiers matched the 1298 previously identified DNMT3A targets and were used to calculate a relative DNMT3A-target expression score; briefly, the $\log_2$ expression of each target gene was scaled to its mean-centered variation across the samples of the dataset, and those normalized expression values were then summed for each sample. In subsequent analyses, this score was also calculated using a limited gene set that included either only those DEGs between in vitro DNMT3A KO and wild-type cells (as assayed by Affymetrix Clariom S human microarray; Ctrl, $n = 3$; KO, $n = 8$) or the intersection between these DEGs and the previously identified DNMT3A targets.

Statistical analysis

Statistical analyses were performed using GraphPad Prism 9.0 (GraphPad Software Inc., La Jolla, CA). Statistical analyses were only performed when the number of replicates was at least three. For comparisons of two groups, a paired or unpaired *t* test was used. Two-tailed *t* tests were performed in all instances unless otherwise specified in the figure legend. For comparisons of three or more groups, a one- or two-way analysis of variance (ANOVA) was used followed by either Dunnett's, Sidak's, or Tukey's multiple comparisons test. A Shapiro- Wilk test was performed to confirm normality before ANOVA, or *t* tests were performed. When the assumption of normality could not be met, nonparametric tests including Mann-Whitney, Kruskal-Wallis, or Wilcoxon signed-rank test were performed instead. In instances where multiple Mann-Whitney tests were performed, a two-stage step-up Benjamini, Krieger, and Yekutieli procedure was applied to account for multiple comparisons, with an FDR of 5%. Survival data were analyzed using a log-rank (Mantel-Cox) test. For all experiments, *P* values of less than 0.05 were considered significant. For DNMT3A expression score statistical analysis, the nonparametric Kruskal-Wallis test and Mann-Whitney *U* test were used to assess significant variation across the patient outcomes defined by the originating study, and plots were generated with ggplot2 (83).

Supplementary Material

Refer to Web version on PubMed Central for supplementary material.

Acknowledgments:

We would like to thank G. Lennon and R. Cross for assistance in FACS purifying cells. Part of the laboratory studies were performed by the Center for Translational Immunology and Immunotherapy (CeTI^2), which is supported by St. Jude.

Funding: Preclinical imaging was performed by the Center for In Vivo Imaging and Therapeutics, which is supported in part by National Institutes of Health (NIH) or National Cancer Institute (NCI) grants P01CA096832 and R50CA211481. Preclinical procedures were performed in collaboration with St. Jude Children's Animal Resource Center. Guide RNA design, validation, and NGS were performed by the Center for Advanced Genome Engineering (CAGE), which is supported in part by NCI P30 CA021765. The Sequencing (Hartwell) Center is supported by NCI/NIH grant P30CA021765. This work was supported by NIH grants 1R01AI114442 to B.Y., 1R01CA237311 to B.Y., R01NS106379–02 to S.G., R01CA173750 to S.G., R01NS121249 to G.K., K99CA256262 to D.H., F31CA250401–01A1 to M.B. and U01AI157189 to S.Q.T.; Immune Tolerance Network UM1AI109565 to B.Y.; the Assisi foundation to B.Y. and G.K.; the Key for a Cure Foundation to B.Y.; and the American Lebanese Syrian Associated Charities (ALSAC) to B.Y., S.G., and G.K.; as well as by St. Jude Comprehensive Cancer Center (SJCCC) Neurobiology and Brain Tumor Program (NBTP), which is funded in part through P30CA021765, to G.K.

REFERENCES AND NOTES

1. Park JH, Geyer MB, Brentjens RJ, CD19-targeted CAR T-cell therapeutics for hematologic malignancies: Interpreting clinical outcomes to date. Blood 127, 3312–3320 (2016). [PubMed: 27207800]
2. Maude SL, Laetsch TW, Buechner J, Rives S, Boyer M, Bittencourt H, Bader P, Verneris MR, Stefanski HE, Myers GD, Qayed M, De Moerloose B, Hiramatsu H, Schlis K, Davis KL, Martin PL, Nemecek ER, Yanik GA, Peters C, Baruchel A, Boissel N, Mechinaud F, Balduzzi A, Krueger J, June CH, Levine BL, Wood P, Taran T, Leung M, Mueller KT, Zhang Y, Sen K, Lebwohl D, Pulsipher MA, Grupp SA, Tisagenlecleucel in children and young adults with B-cell lymphoblastic leukemia. N. Engl. J. Med. 378, 439–448 (2018). [PubMed: 29385370]
3. Fraietta JA, Lacey SF, Orlando EJ, Pruteanu-Malinici I, Gohil M, Lundh S, Boesteanu AC, Wang Y, O'Connor RS, Hwang WT, Pequignot E, Ambrose DE, Zhang C, Wilcox N, Bedoya F, Dorfmeier C, Chen F, Tian L, Parakandi H, Gupta M, Young RM, Johnson FB, Kulikovskaya I, Liu L, Xu J, Kassim SH, Davis MM, Levine BL, Frey NV, Siegel DL, Huang AC, Wherry EJ, Bitter H, Brogdon JL, Porter DL, June CH, Melenhorst JJ, Determinants of response and resistance to CD19 chimeric antigen receptor (CAR) T cell therapy of chronic lymphocytic leukemia. Nat. Med. 24, 563–571 (2018). [PubMed: 29713085]
4. Ahmed N, Brawley VS, Hegde M, Robertson C, Ghazi A, Gerken C, Liu E, Dakhova O, Ashoori A, Corder A, Gray T, Wu MF, Liu H, Hicks J, Rainusso N, Dotti G, Mei Z, Grilley B, Gee A, Rooney CM, Brenner MK, Heslop HE, Wels WS, Wang LL, Anderson P, Gottschalk S, Human epidermal growth factor receptor 2 (HER2)-specific chimeric antigen receptor-modified T cells for the immunotherapy of HER2-positive sarcoma. J. Clin. Oncol. 33, 1688–1696 (2015). [PubMed: 25800760]
5. Beatty GL, O'Hara MH, Lacey SF, Torigian DA, Nazimuddin F, Chen F, Kulikovskaya IM, Soulen MC, McGarvey M, Nelson AM, Gladney WL, Levine BL, Melenhorst JJ, Plesa G, June CH, Activity of mesothelin-specific chimeric antigen receptor t cells against pancreatic carcinoma metastases in a phase 1 trial. Gastroenterology 155, 29–32 (2018). [PubMed: 29567081]
6. Thistlethwaite FC, Gilham DE, Guest RD, Rothwell DG, Pillai M, Burt DJ, Byatte AJ, Kirillova N, Valle JW, Sharma SK, Chester KA, Westwood NB, Halford SER, Nabarro S, Wan S, Austin E, Hawkins RE, The clinical efficacy of first-generation carcinoembryonic antigen (CEACAM5)-specific CAR T cells is limited by poor persistence and transient pre-conditioning-dependent respiratory toxicity. Cancer Immunol. 66, 1425–1436 (2017).
7. Heczey A, Louis CU, Savoldo B, Dakhova O, Durett A, Grilley B, Liu H, Wu MF, Mei Z, Gee A, Mehta B, Zhang H, Mahmood N, Tashiro H, Heslop HE, Dotti G, Rooney CM, Brenner MK, CAR T cells administered in combination with lymphodepletion and PD-1 inhibition to patients with neuroblastoma. Mol. Ther. 25, 2214–2224 (2017). [PubMed: 28602436]
8. O'Rourke DM, Nasrallah MP, Desai A, Melenhorst JJ, Mansfield K, Morrissette JJD, Martinez-Lage M, Brem S, Maloney E, Shen A, Isaacs R, Mohan S, Plesa G, Lacey SF, Navenot J-M, Zheng

Z, Levine BL, Okada H, June CH, Brogdon JL, Maus MV, A single dose of peripherally infused EGFRvIII-directed CAR T cells mediates antigen loss and induces adaptive resistance in patients with recurrent glioblastoma. Sci. Transl. Med. 9, eaaa0984 (2017).

9. Brown CE, Alizadeh D, Starr R, Weng L, Wagner JR, Naranjo A, Ostberg JR, Suzette Blanchard M, Kilpatrick J, Simpson J, Kurien A, Priceman SJ, Wang X, Harshbarger TL, D'Apuzzo M, Ressler JA, Jensen MC, Barish ME, Chen M, Portnow J, Forman SJ, Badie B, Regression of glioblastoma after chimeric antigen receptor T-cell therapy. N. Engl. J. Med. 375, 2561–2569 (2016). [PubMed: 28029927]
10. Maude SL, Frey N, Shaw PA, Aplenc R, Barrett DM, Bunin NJ, Chew A, Gonzalez VE, Zheng Z, Lacey SF, Mahnke YD, Melenhorst JJ, Rheingold SR, Shen A, Teachey DT, Levine BL, June CH, Porter DL, Grupp SA, Chimeric antigen receptor T cells for sustained remissions in leukemia. N. Engl. J. Med. 371, 1507–1517 (2014). [PubMed: 25317870]
11. Long AH, Haso WM, Shern JF, Wanhainen KM, Murgai M, Ingaramo M, Smith JP, Walker AJ, Eric Kohler M, Venkateshwara VR, Kaplan RN, Patterson GH, Fry TJ, Orentas RJ, Mackall CL, 4–1BB costimulation ameliorates T cell exhaustion induced by tonic signaling of chimeric antigen receptors. Nat. Med. 21, 581–590 (2015). [PubMed: 25939063]
12. Ghosh A, Smith M, James SE, Davila ML, Velardi E, Argyropoulos KV, Gunset G, Perna F, Kreines FM, Levy ER, Lieberman S, Jay H, Tuckett AZ, Zakrzewski JL, Tan L, Young LF, Takvorian K, Dudakov JA, Jenq RR, Hanash AM, Motta ACF, Murphy GF, Liu C, Schietinger A, Sadelain M, van den Brink MRM, Donor CD19 CAR T cells exert potent graft-versus-lymphoma activity with diminished graft-versus-host activity. Nat. Med. 23, 242–249 (2017). [PubMed: 28067900]
13. Pauken KE, Sammons MA, Odorizzi PM, Manne S, Godec J, Khan O, Drake AM, Chen Z, Sen DR, Kurachi M, Anthony Barnitz R, Bartman C, Bengsch B, Huang AC, Schenkel JM, Vahedi G, Nicholas Haining W, Berger SL, John Wherry E, Epigenetic stability of exhausted T cells limits durability of reinvigoration by PD-1 blockade. Science 354, 1160–1165 (2016). [PubMed: 27789795]
14. Sen DR, Kaminski J, Anthony Barnitz R, Kurachi M, Gerdemann U, Yates KB, Tsao H-W, Godec J, La Fleur MW, Brown FD, Tonnerre P, Chung RT, Tully DC, Allen TM, Frahm N, Lauer GM, John Wherry E, Yosef N, Nicholas Haining W, The epigenetic landscape of T cell exhaustion. Science 354, 1165–1169 (2016). [PubMed: 27789799]
15. Ghoneim HE, Fan Y, Moustaki A, Abdelsamed HA, Dash P, Dogra P, Carter R, Awad W, Neale G, Thomas PG, Youngblood B, De novo epigenetic programs inhibit PD-1 blockade-mediated T cell rejuvenation. Cell 170, 142–157.e19 (2017). [PubMed: 28648661]
16. Youngblood B, Noto A, Porichis F, Akondy RS, Ndhlovu ZM, Austin JW, Bordi R, Procopio FA, Miura T, Allen TM, Sidney J, Sette A, Walker BD, Ahmed R, Boss JM, Sékaly R-P, Kaufmann DE, Cutting edge: Prolonged exposure to HIV reinforces a poised epigenetic program for PD-1 expression in virus-specific CD8 T cells. J. Immunol. 191, 540–544 (2013). [PubMed: 23772031]
17. Youngblood B, Oestreich KJ, Ha S-J, Duraiswamy J, Akondy RS, West EE, Wei Z, Lu P, Austin JW, Riley JL, Boss JM, Ahmed R, Chronic virus infection enforces demethylation of the locus that encodes PD-1 in antigen-specific CD8(+) T cells. Immunity 35, 400–412 (2011). [PubMed: 21943489]
18. Nakayama-Hosoya K, Ishida T, Youngblood B, Nakamura H, Hosoya N, Koga M, Koibuchi T, Iwamoto A, Kawana-Tachikawa A, Epigenetic repression of interleukin 2 expression in senescent CD4+ T cells during chronic HIV type 1 infection. J. Infect. Dis. 211, 28–39 (2015). [PubMed: 25001463]
19. Scharer CD, Barwick BG, Youngblood BA, Ahmed R, Boss JM, Global DNA methylation remodeling accompanies CD8 T cell effector function. J. Immunol. 191, 3419–3429 (2013). [PubMed: 23956425]
20. Youngblood B, Wherry EJ, Ahmed R, Acquired transcriptional programming in functional and exhausted virus-specific CD8 T cells. Curr. Opin. HIV AIDS 7, 50–57 (2012). [PubMed: 22134341]
21. Abdelsamed HA, Moustaki A, Fan Y, Dogra P, Ghoneim HE, Zebley CC, Triplett BM, Sekaly R-P, Youngblood B, Human memory CD8 T cell effector potential is epigenetically preserved during in vivo homeostasis. J. Exp. Med. 214, 1593–1606 (2017). [PubMed: 28490440]

22. Ahn E, Youngblood B, Lee J, Lee J, Sarkar S, Ahmed R, Demethylation of the PD-1 promoter is imprinted during the effector phase of CD8 T cell exhaustion. J. Virol. 90, 8934–8946 (2016). [PubMed: 27466420]
23. Zebley CC, Gottschalk S, Youngblood B, Rewriting history: Epigenetic reprogramming of CD8(+) T cell differentiation to enhance immunotherapy. Trends Immunol. 41, 665–675 (2020). [PubMed: 32624330]
24. Liao J, Karnik R, Gu H, Ziller MJ, Clement K, Tsankov AM, Akopian V, Gifford CA, Donaghey J, Galonska C, Pop R, Reyon D, Tsai SQ, Mallard W, Joung JK, Rinn JL, Gnirke A, Meissner A, Targeted disruption of DNMT1, DNMT3A and DNMT3B in human embryonic stem cells. Nat. Genet. 47, 469–478 (2015). [PubMed: 25822089]
25. Krenciute G, Prinzing BL, Yi Z, Wu MF, Liu H, Dotti G, Balyasnikova IV, Gottschalk S, Transgenic expression of IL15 improves antiglioma activity of IL13Rα2-CAR T cells but results in antigen loss variants. Cancer Immunol. Res. 5, 571–581 (2017). [PubMed: 28550091]
26. Mata M, Gerken C, Nguyen P, Krenciute G, Spencer DM, Gottschalk S, Inducible activation of MyD88 and CD40 in CAR T cells results in controllable and potent antitumor activity in preclinical solid tumor models. Cancer Discov. 7, 1306–1319 (2017). [PubMed: 28801306]
27. Ahmed N, Ratnayake M, Savoldo B, Perlaky L, Dotti G, Wels WS, Bhattacharjee MB, Gilbertson RJ, Shine HD, Weiss HL, Rooney CM, Heslop HE, Gottschalk S, Regression of experimental medulloblastoma following transfer of HER2-specific T cells. Cancer Res. 67, 5957–5964 (2007). [PubMed: 17575166]
28. Krenciute G, Krebs S, Torres D, Wu MF, Liu H, Dotti G, Li XN, Lesniak MS, Balyasnikova IV, Gottschalk S, Characterization and functional analysis of scFv-based chimeric antigen receptors to redirect T cells to IL13Rα2-positive glioma. Mol. Ther. 24, 354–363 (2016). [PubMed: 26514825]
29. Yi Z, Prinzing BL, Cao F, Gottschalk S, Krenciute G, Optimizing EphA2-CAR T cells for the adoptive immunotherapy of glioma. Mol. Ther. Methods Clin. Dev. 9, 70–80 (2018). [PubMed: 29552579]
30. Roychoudhuri R, Clever D, Li P, Wakabayashi Y, Quinn KM, Klebanoff CA, Ji Y, Sukumar M, Eil RL, Yu Z, Spolski R, Palmer DC, Pan JH, Patel SJ, Macallan DC, Fabozzi G, Shih HY, Kanno Y, Muto A, Zhu J, Gattinoni L, O'Shea JJ, Okkenhaug K, Igarashi K, Leonard WJ, Restifo NP, BACH2 regulates CD8(+) T cell differentiation by controlling access of AP-1 factors to enhancers. Nat. Immunol. 17, 851–860 (2016). [PubMed: 27158840]
31. Kaech SM, Cui W, Transcriptional control of effector and memory CD8+ T cell differentiation. Nat. Rev. Immunol. 12, 749–761 (2012). [PubMed: 23080391]
32. Chen Y, Zander R, Khatun A, Schauder DM, Cui W, Transcriptional and epigenetic regulation of effector and memory CD8 T cell differentiation. Front. Immunol. 9, 2826 (2018). [PubMed: 30581433]
33. Alfei F, Kanev K, Hofmann M, Wu M, Ghoneim HE, Roelli P, Utzschneider DT, von Hoesslin M, Cullen JG, Fan Y, Eisenberg V, Wohlleber D, Steiger K, Merkler D, Delorenzi M, Knolle PA, Cohen CJ, Thimme R, Youngblood B, Zehn D, TOX reinforces the phenotype and longevity of exhausted T cells in chronic viral infection. Nature 571, 265–269 (2019). [PubMed: 31207605]
34. Khan O, Giles JR, McDonald S, Manne S, Ngiow SF, Patel KP, Werner MT, Huang AC, Alexander KA, Wu JE, Attanasio J, Yan P, George SM, Bengsch B, Staupe RP, Donahue G, Xu W, Amaravadi RK, Xu X, Karakousis GC, Mitchell TC, Schuchter LM, Kaye J, Berger SL, Wherry EJ, TOX transcriptionally and epigenetically programs CD8(+) T cell exhaustion. Nature 571, 211–218 (2019). [PubMed: 31207603]
35. Scott AC, Dundar F, Zumbo P, Chandran SS, Klebanoff CA, Shakiba M, Trivedi P, Menocal L, Appleby H, Camara S, Zamarin D, Walther T, Snyder A, Femia MR, Comen EA, Wen HY, Hellmann MD, Anandasabapathy N, Liu Y, Altorki NK, Lauer P, Levy O, Glickman MS, Kaye J, Betel D, Philip M, Schietinger A, TOX is a critical regulator of tumour-specific T cell differentiation. Nature 571, 270–274 (2019). [PubMed: 31207604]
36. Abdelsamed HA, Zebley CC, Nguyen H, Rutishauser RL, Fan Y, Ghoneim HE, Crawford JC, Alfei F, Alli S, Ribeiro SP, Castellaw AH, McGargill MA, Jin H, Boi SK, Speake C, Serti E, Turka LA, Busch ME, Stone M, Deeks SG, Sekaly RP, Zehn D, James EA, Nepom GT, Youngblood B, Beta cell-specific CD8+ T cells maintain stem cell memory-associated epigenetic programs during type 1 diabetes. Nat. Immunol. 21, 578–587 (2020). [PubMed: 32231298]

37. Schultz L, Mackall C, Driving CAR T cell translation forward. Sci. Transl. Med. 11, eaaw2127 (2019).
38. Mueller KT, Maude SL, Porter DL, Frey N, Wood P, Han X, Waldron E, Chakraborty A, Awasthi R, Levine BL, Melenhorst JJ, Grupp SA, June CH, Lacey SF, Cellular kinetics of CTL019 in relapsed/refractory B-cell acute lymphoblastic leukemia and chronic lymphocytic leukemia. Blood 130, 2317–2325 (2017). [PubMed: 28935694]
39. Porter DL, Hwang WT, Frey NV, Lacey SF, Shaw PA, Loren AW, Bagg A, Marcucci KT, Shen A, Gonzalez V, Ambrose D, Grupp SA, Chew A, Zheng Z, Milone MC, Levine BL, Melenhorst JJ, June CH, Chimeric antigen receptor T cells persist and induce sustained remissions in relapsed refractory chronic lymphocytic leukemia. Sci. Transl. Med. 7, 303ra139 (2015).
40. Feucht J, Sun J, Eyquem J, Ho YJ, Zhao Z, Leibold J, Dobrin A, Cabriolu A, Hamieh M, Sadelain M, Calibration of CAR activation potential directs alternative T cell fates and therapeutic potency. Nat. Med. 25, 82–88 (2019). [PubMed: 30559421]
41. Sommermeyer D, Hudecek M, Kosasih PL, Gogishvili T, Maloney DG, Turtle CJ, Riddell SR, Chimeric antigen receptor-modified T cells derived from defined CD8+ and CD4+ subsets confer superior antitumor reactivity in vivo. Leukemia 30, 492–500 (2016). [PubMed: 26369987]
42. Gattinoni L, Lugli E, Ji Y, Pos Z, Paulos CM, Quigley MF, Almeida JR, Gostick E, Yu Z, Carpenito C, Wang E, Douek DC, Price DA, June CH, Marincola FM, Roederer M, Restifo NP, A human memory T cell subset with stem cell-like properties. Nat. Med. 17, 1290–1297 (2011). [PubMed: 21926977]
43. Krishna S, Lowery FJ, Copeland AR, Bahadiroglu E, Mukherjee R, Jia L, Anibal JT, Sachs A, Adebola SO, Gurusamy D, Yu Z, Hill V, Gartner JJ, Li YF, Parkhurst M, Paria B, Kvistborg P, Kelly MC, Goff SL, Altan-Bonnet G, Robbins PF, Rosenberg SA, Stem-like CD8 T cells mediate response of adoptive cell immunotherapy against human cancer. Science 370, 1328–1334 (2020). [PubMed: 33303615]
44. Park JH, Rivière I, Gonen M, Wang X, Sénéchal B, Curran KJ, Sauter C, Wang Y, Santomasso B, Mead E, Roshal M, Maslak P, Davila M, Brentjens RJ, Sadelain M, Long-term follow-up of CD19 CAR therapy in acute lymphoblastic leukemia. N. Engl. J. Med. 378, 449–459 (2018). [PubMed: 29385376]
45. Sade-Feldman M, Yizhak K, Bjorgaard SL, Ray JP, de Boer CG, Jenkins RW, Lieb DJ, Chen JH, Frederick DT, Barzily-Rokni M, Freeman SS, Reuben A, Hoover PJ, Villani A-C, Ivanova E, Portell A, Lizotte PH, Aref AR, Eliane J-P, Hammond MR, Vitzthum H, Blackmon SM, Li B, Gopalakrishnan V, Reddy SM, Cooper ZA, Paweletz CP, Barbie DA, Stemmer-Rachamimov A, Flaherty KT, Wargo JA, Boland GM, Sullivan RJ, Getz G, Hacohen N, Defining T cell states associated with response to checkpoint immunotherapy in melanoma. Cell 175, 998–1013.e20 (2018). [PubMed: 30388456]
46. Fraietta JA, Nobles CL, Sammons MA, Lundh S, Carty SA, Reich TJ, Cogdill AP, Morrissette JJD, DeNizio JE, Reddy S, Hwang Y, Gohil M, Kulikovskaya I, Nazimuddin F, Gupta M, Chen F, Everett JK, Alexander KA, Lin-Shiao E, Gee MH, Liu X, Young RM, Ambrose D, Wang Y, Xu J, Jordan MS, Marcucci KT, Levine BL, Garcia KC, Zhao Y, Kalos M, Porter DL, Kohli RM, Lacey SF, Berger SL, Bushman FD, June CH, Melenhorst JJ, Disruption of TET2 promotes the therapeutic efficacy of CD19-targeted T cells. Nature 558, 307–312 (2018). [PubMed: 29849141]
47. Lynn RC, Weber EW, Sotillo E, Gennert D, Xu P, Good Z, Anbunathan H, Lattin J, Jones R, Tieu V, Nagaraja S, Granja J, de Bourcy CFA, Majzner R, Satpathy AT, Quake SR, Monje M, Chang HY, Mackall CL, c-Jun overexpression in CAR T cells induces exhaustion resistance. Nature 576, 293–300 (2019). [PubMed: 31802004]
48. Moskophidis D, Lechner F, Pircher H, Zinkernagel RM, Virus persistence in acutely infected immunocompetent mice by exhaustion of antiviral cytotoxic effector T cells. Nature 362, 758–761 (1993). [PubMed: 8469287]
49. Zajac AJ, Blattman JN, Murali-Krishna K, Sourdive DJD, Suresh M, Altman JD, Ahmed R, Viral immune evasion due to persistence of activated T cells without effector function. J. Exp. Med. 188, 2205–2213 (1998). [PubMed: 9858507]
50. Hui E, Cheung J, Zhu J, Su X, Taylor MJ, Wallweber HA, Sasmal DK, Huang J, Kim JM, Mellman I, Vale RD, T cell costimulatory receptor CD28 is a primary target for PD-1-mediated inhibition. Science 355, 1428–1433 (2017). [PubMed: 28280247]

51. Kamphorst AO, Wieland A, Nasti T, Yang S, Zhang R, Barber DL, Konieczny BT, Daugherty CZ, Koenig L, Yu K, Sica GL, Sharpe AH, Freeman GJ, Blazar BR, Turka LA, Owonikoko TK, Pillai RN, Ramalingam SS, Araki K, Ahmed R, Rescue of exhausted CD8 T cells by PD-1-targeted therapies is CD28-dependent. Science 355, 1423–1427 (2017). [PubMed: 28280249]
52. Brooks DG, Trifilo MJ, Edelmann KH, Teyton L, McGavern DB, Oldstone MBA, Interleukin-10 determines viral clearance or persistence in vivo. Nat. Med. 12, 1301–1309 (2006). [PubMed: 17041596]
53. Fujii S, Shimizu K, Shimizu T, Lotze MT, Interleukin-10 promotes the maintenance of antitumor CD8(+) T-cell effector function in situ. Blood 98, 2143–2151 (2001). [PubMed: 11568001]
54. Guo Y, Xie YQ, Gao M, Zhao Y, Franco F, Wenes M, Siddiqui I, Bevilacqua A, Wang H, Yang H, Feng B, Xie X, Sabatel CM, Tschumi B, Chaiboonchoe A, Wang Y, Li W, Xiao W, Held W, Romero P, Ho PC, Tang L, Metabolic reprogramming of terminally exhausted CD8(+) T cells by IL-10 enhances anti-tumor immunity. Nat. Immunol. 22, 746–756 (2021). [PubMed: 34031618]
55. Ley TJ, Ding L, Walter MJ, McLellan MD, Lamprecht T, Larson DE, Kandoth C, Payton JE, Baty J, Welch J, Harris CC, Lichti CF, Townsend RR, Fulton RS, Dooling DJ, Koboldt DC, Schmidt H, Zhang Q, Osborne JR, Lin L, O'Laughlin M, McMichael JF, Delehaunty KD, McGrath SD, Fulton LA, Magrini VJ, Vickery TL, Hundal J, Cook LL, Conyers JJ, Swift GW, Reed JP, Alldredge PA, Wylie T, Walker J, Kalicki J, Watson MA, Heath S, Shannon WD, Varghese N, Nagarajan R, Westervelt P, Tomasson MH, Link DC, Graubert TA, DiPersio JF, Mardis ER, Wilson RK, DNMT3A mutations in acute myeloid leukemia. N. Engl. J. Med. 363, 2424–2433 (2010). [PubMed: 21067377]
56. Walter MJ, Ding L, Shen D, Shao J, Grillot M, McLellan M, Fulton R, Schmidt H, Kalicki-Veizer J, O'Laughlin M, Kandoth C, Baty J, Westervelt P, DiPersio JF, Mardis ER, Wilson RK, Ley TJ, Graubert TA, Recurrent DNMT3A mutations in patients with myelodysplastic syndromes. Leukemia 25, 1153–1158 (2011). [PubMed: 21415852]
57. Kramer AC, Kothari A, Wilson WC, Celik H, Nikitas J, Mallaney C, Ostrander EL, Eultgen E, Martens A, Valentine MC, Young AL, Druley TE, Figueroa ME, Zhang B, Challen GA, Dnmt3a regulates T-cell development and suppresses T-ALL transformation. Leukemia 31, 2479–2490 (2017). [PubMed: 28321121]
58. Youngblood B, Hale JS, Kissick HT, Ahn E, Xu X, Wieland A, Araki K, West EE, Ghoneim HE, Fan Y, Dogra P, Davis CW, Konieczny BT, Antia R, Cheng X, Ahmed R, Effector CD8 T cells dedifferentiate into long-lived memory cells. Nature 552, 404–409 (2017). [PubMed: 29236683]
59. Tovy A, Reyes JM, Gundry MC, Brunetti L, Lee-Six H, Petljak M, Park HJ, Guzman AG, Rosas C, Jeffries AR, Baple E, Mill J, Crosby AH, Sency V, Xin B, Machado HE, Castillo D, Weitzel JN, Li W, Stratton MR, Campbell PJ, Wang H, Sanders MA, Goodell MA, Tissue-biased expansion of DNMT3A-mutant clones in a mosaic individual is associated with conserved epigenetic erosion. Cell Stem Cell 27, 326–335.e4 (2020). [PubMed: 32673568]
60. Lange S, Sand LGL, Bell M, Patil SL, Langfitt D, Gottschalk S, A chimeric GM-CSF/IL18 receptor to sustain CAR T-cell function. Cancer Discov. 11, 1661–1671 (2021). [PubMed: 33563660]
61. Hu B, Ren J, Luo Y, Keith B, Young RM, Scholler J, Zhao Y, June CH, Augmentation of antitumor immunity by human and mouse CAR T cells secreting IL-18. Cell Rep. 20, 3025–3033 (2017). [PubMed: 28954221]
62. Chow KK, Naik S, Kakarla S, Brawley VS, Shaffer DR, Yi Z, Rainusso N, Wu MF, Liu H, Kew Y, Grossman RG, Powell S, Lee D, Ahmed N, Gottschalk S, T cells redirected to EphA2 for the immunotherapy of glioblastoma. Mol. Ther. 21, 629–637 (2013). [PubMed: 23070117]
63. Iacobucci I, Li Y, Roberts KG, Dobson SM, Kim JC, Payne-Turner D, Harvey RC, Valentine M, McCastlain K, Easton J, Yergeau D, Janke LJ, Shao Y, Chen IML, Rusch M, Zandi S, Kornblau SM, Konopleva M, Jabbour E, Paietta EM, Rowe JM, Pui CH, Gastier-Foster J, Gu Z, Reshmi S, Loh ML, Racevskis J, Tallman MS, Wiernik PH, Litzow MR, Willman CL, McPherson JD, Downing JR, Zhang J, Dick JE, Hunger SP, Mullighan CG, Truncating erythropoietin receptor rearrangements in acute lymphoblastic leukemia. Cancer Cell 29, 186–200 (2016). [PubMed: 26859458]

64. Chockley P, Patil SL, Gottschalk S, Transient blockade of TBK1/IKKε allows efficient transduction of primary human natural killer cells with vesicular stomatitis virus G-pseudotyped lentiviral vectors. Cytotherapy 23, 787–792 (2021). [PubMed: 34119434]

65. Ahmed N, Salsman VS, Yvon E, Louis CU, Perlaky L, Wels WS, Dishop MK, Kleinerman EE, Pule M, Rooney CM, Heslop HE, Gottschalk S, Immunotherapy for osteosarcoma: Genetic modification of T cells overcomes low levels of tumor antigen expression. Mol. Ther. 17, 1779–1787 (2009). [PubMed: 19532139]

66. Li W, Guo L, Rathi P, Marinova E, Gao X, Wu MF, Liu H, Dotti G, Gottschalk S, Metelitsa LS, Heczey A, Redirecting T cells to glypican-3 with 4–1BB zeta chimeric antigen receptors results in Th1 polarization and potent antitumor activity. Hum. Gene Ther. 28, 437–448 (2017). [PubMed: 27530312]

67. Shaffer DR, Savoldo B, Yi Z, Chow KKH, Kakarla S, Spencer DM, Dotti G, Wu MF, Liu H, Kenney S, Gottschalk S, T cells redirected against CD70 for the immunotherapy of CD70-positive malignancies. Blood 117, 4304–4314 (2011). [PubMed: 21304103]

68. Chan WK, Suwannasaen D, Throm RE, Li Y, Eldridge PW, Houston J, Gray JT, Pui CH, Leung W, Chimeric antigen receptor-redirected CD45RA-negative T cells have potent antileukemia and pathogen memory response without graft-versus-host activity. Leukemia 29, 387–395 (2015). [PubMed: 24888271]

69. Imai C, Mihara K, Andreansky M, Nicholson IC, Pui CH, Geiger TL, Campana D, Chimeric receptors with 4–1BB signaling capacity provoke potent cytotoxicity against acute lymphoblastic leukemia. Leukemia 18, 676–684 (2004). [PubMed: 14961035]

70. Bauler M, Roberts JK, Wu CC, Fan B, Ferrara F, Yip BH, Diao S, Kim YI, Moore J, Zhou S, Wielgosz MM, Ryu B, Throm RE, Production of lentiviral vectors using suspension cells grown in serum-free media. Mol. Ther. Methods Clin. Dev. 17, 58–68 (2020). [PubMed: 31890741]

71. Connelly JP, Pruett-Miller SM, CRIS.py: A versatile and high-throughput analysis program for CRISPR-based genome editing. Sci. Rep. 9, 4194 (2019). [PubMed: 30862905]

72. Velasquez MP, Torres D, Iwahori K, Kakarla S, Arber C, Rodriguez-Cruz T, Szoor A, Bonifant CL, Gerken C, Cooper LJN, Song XT, Gottschalk S, T cells expressing CD19-specific engager molecules for the immunotherapy of CD19-positive malignancies. Sci. Rep. 6, 27130 (2016). [PubMed: 27255991]

73. Robinson JT, Thorvaldsdóttir H, Winckler W, Guttman M, Lander ES, Getz G, Mesirov JP, Integrative genomics viewer. Nat. Biotechnol. 29, 24–26 (2011). [PubMed: 21221095]

74. Wu H, Xu T, Feng H, Chen L, Li B, Yao B, Qin Z, Jin P, Conneely KN, Detection of differentially methylated regions from whole-genome bisulfite sequencing data without replicates. Nucleic Acids Res. 43, e141 (2015). [PubMed: 26184873]

75. Xi Y, Li W, BSMAP: Whole genome bisulfite sequence MAPping program. BMC Bioinformatics 10, 232 (2009). [PubMed: 19635165]

76. Sun D, Xi Y, Rodriguez B, Park H, Tong P, Meong M, Goodell MA, Li W, MOABS: Model based analysis of bisulfite sequencing data. Genome Biol. 15, R38 (2014). [PubMed: 24565500]

77. Subramanian A, Tamayo P, Mootha VK, Mukherjee S, Ebert BL, Gillette MA, Paulovich A, Pomeroy SL, Golub TR, Lander ES, Mesirov JP, Gene set enrichment analysis: A knowledge-based approach for interpreting genome-wide expression profiles. Proc. Natl. Acad. Sci. U.S.A. 102, 15545–15550 (2005). [PubMed: 16199517]

78. Fonseca R, Beura LK, Quarnstrom CF, Ghoneim HE, Fan Y, Zebley CC, Scott MC, Fares-Frederickson NJ, Wijeyesinghe S, Thompson EA, Borges da Silva H, Vezys V, Youngblood B, Masopust D, Developmental plasticity allows outside-in immune responses by resident memory T cells. Nat. Immunol. 21, 412–421 (2020). [PubMed: 32066954]

79. Malta TM, Sokolov A, Gentles AJ, Burzykowski T, Poisson L, Weinstein JN, Kamińska B, Huelsken J, Omberg L, Gevaert O, Colaprico A, Czerwińska P, Mazurek S, Mishra L, Heyn H, Krasnitz A, Godwin AK, Lazar AJ, Machine learning identifies stemness features associated with oncogenic dedifferentiation. Cell 173, 338–354.e15 (2018). [PubMed: 29625051]

80. Sokolov A, Carlin DE, Paull EO, Baertsch R, Stuart JM, Pathway-based genomics prediction using generalized elastic net. PLoS Comput. Biol. 12, e1004790 (2016). [PubMed: 26960204]

81. Robinson MD, Carthy DJM, Smyth GK, edgeR: A Bioconductor package for differential expression analysis of digital gene expression data. Bioinformatics 26, 139–140 (2010). [PubMed: 19910308]

82. Ritchie ME, Phipson B, Wu D, Hu Y, Law CW, Shi W, Smyth GK, limma powers differential expression analyses for RNA-sequencing and microarray studies. Nucleic Acids Res. 43, e47 (2015). [PubMed: 25605792]

83. Wickham H, ggplot2: Elegant Graphics for Data Analysis (Springer, 2016).

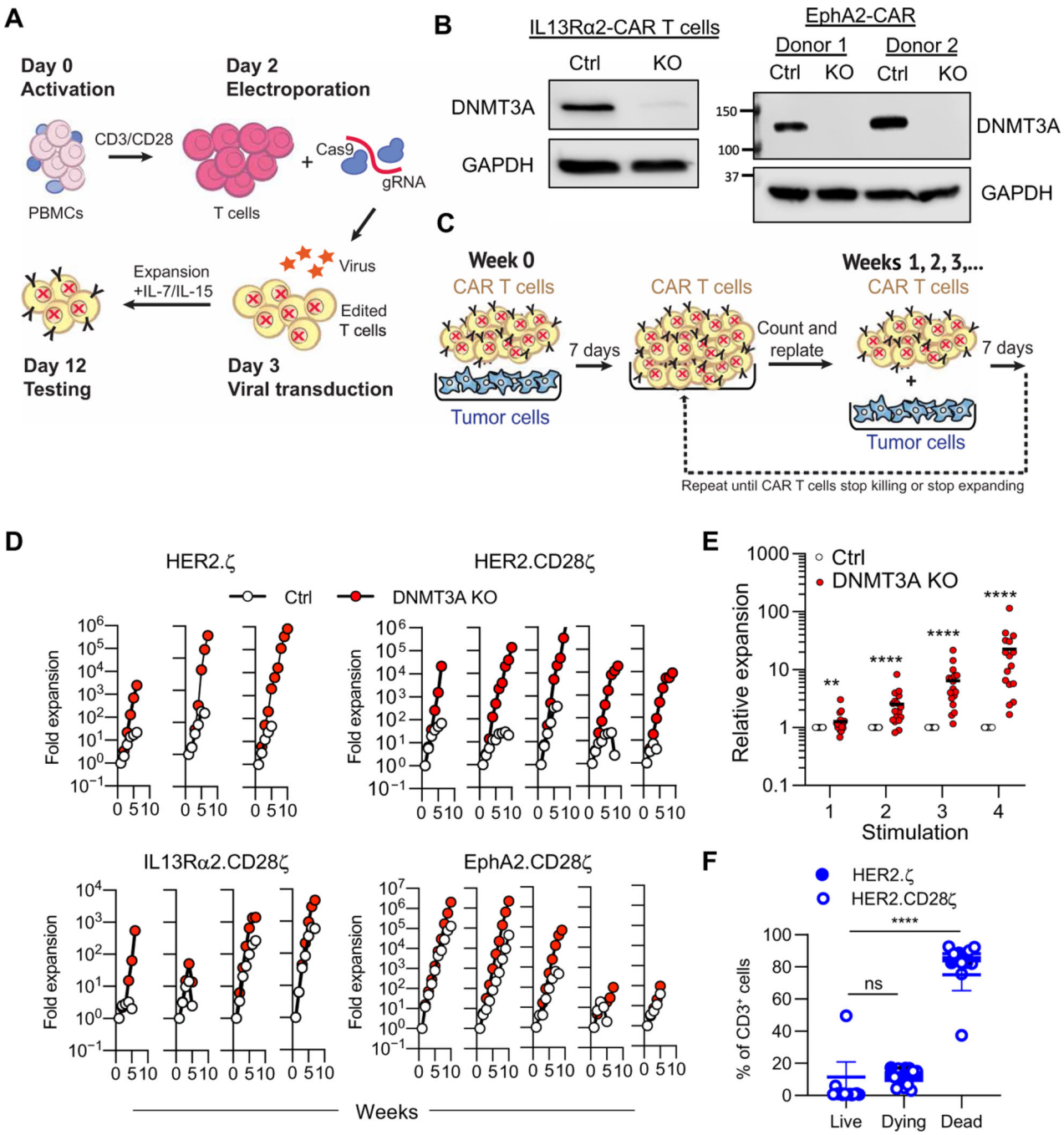

Fig. 1. DNMT3A deletion enhances CAR T cell expansion during repeat stimulation in vitro.

(**A**) Human T cells were transduced with retroviral vectors encoding CARs and DNMT3A was deleted using CRISPR-Cas9. gRNA, guide RNA. (**B**) A Western blot of DNMT3A protein expression in control (Ctrl) and DNMT3A KO (g2) IL13Rα2- and EphA2-CAR T cells is shown. GAPDH was used as a loading control; two independent donors are shown. (**C**) The schematic of the repeat stimulation coculture assay is shown. (**D**) Ctrl and DNMT3A KO CAR T cell expansion was measured after weekly stimulations with U373 cells for HER2.ζ-CAR ($n = 3$), HER2.CD28ζ-CAR ($n = 5$), IL13Rα2.CD28ζ-CAR ($n = 4$),

or EphA2. CD28ζ-CAR ($n = 5$) T cells. (**E**) Expansion of DNMT3A KO relative to Ctrl CAR T cells at each of the first four stimulations is shown ($n = 17$). Data were analyzed using Mann-Whitney tests with a two-stage step-up Benjamini, Krieger, and Yekutieli procedure applied to account for multiple comparisons and a false discovery rate (FDR) set to 5%. Horizontal bars indicate means. (**F**) After the fourth stimulation with tumor cells, DNMT3A KO HER.ζ- or HER2.CD28ζ-CAR T cells were sorted and plated without antigen (U373 tumor cells) in the presence or absence of IL-15. After 7 days, T cells were stained with a viability dye [LIVE/DEAD Aqua (LDA)] and annexin V and classified as live (LDA^-, annexin V^-), preapoptotic/dying (LDA^-, annexin V^+), or dead (LDA^+, annexin V^+) using flow cytometry. Data are presented as means ± SEM. Data were analyzed using a Kruskal-Wallis test with Dunn's multiple comparisons test. ns, not significant; $^{**}P < 0.01$ and $^{****}P < 0.0001$.

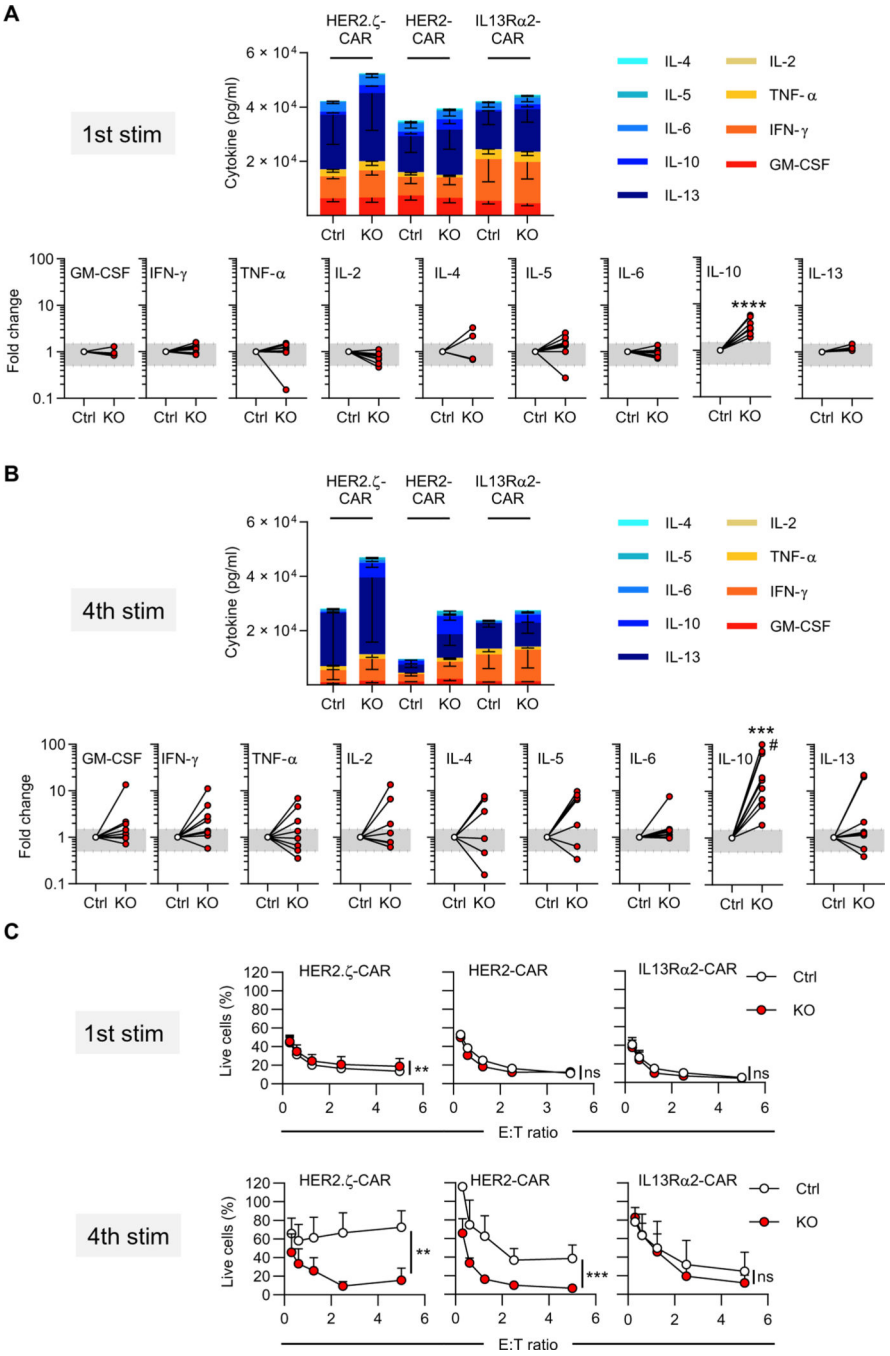

Fig. 2. DNMT3A KO CAR T cells exhibit sustained cytokine secretion and cytolytic activity after repeat antigen stimulation.

To assess T_H1 and T_H2 cytokine production, Ctrl and DNMT3A KO CAR T cells were stimulated as described in Fig. 1C. Cell culture supernatants were harvested 24 hours after each stimulation, and a multiplex assay was used to determine cytokine production. (**A**) A summary of T_H1 and T_H2 cytokine production and fold change in cytokine production of Ctrl versus DNMT3A KO CAR T cells after the first stimulation with tumor cells is shown. Data are presented as means ± SEM (n = 3 per CAR construct). Gray boxes indicate a

fold change from 0.5 to 1.5. Data were analyzed using a Wilcoxon signed-rank test. (**B**) Cytokine production as described above was measured after the fourth stimulation with fresh tumor cells. Data are presented as means ± SEM (n = 3 per CAR construct). Gray boxes indicate a fold change from 0.5 to 1.5. Data were analyzed using a Wilcoxon signed-rank test; #: value was set to 100-fold (actual value: 174-fold). (**C**) A 24-hour MTS assay was used to assess the cytolytic activity of Ctrl and DNMT3A KO HER.ζ-, HER2.CD28ζ-, and IL13Rα2.CD28ζ-CAR T cells at their first (1st stim) or fourth (4th stim) exposure to tumor cells at the indicated effector:target (E:T) ratios. Data are presented as means ± SEM (n = 3 to 5 per group). Data were analyzed using a two-tailed paired t test. All statistical tests compared Ctrl to DNMT3A KO; ns, not significant; ** $P < 0.01$, *** $P < 0.001$, and **** $P < 0.0001$.

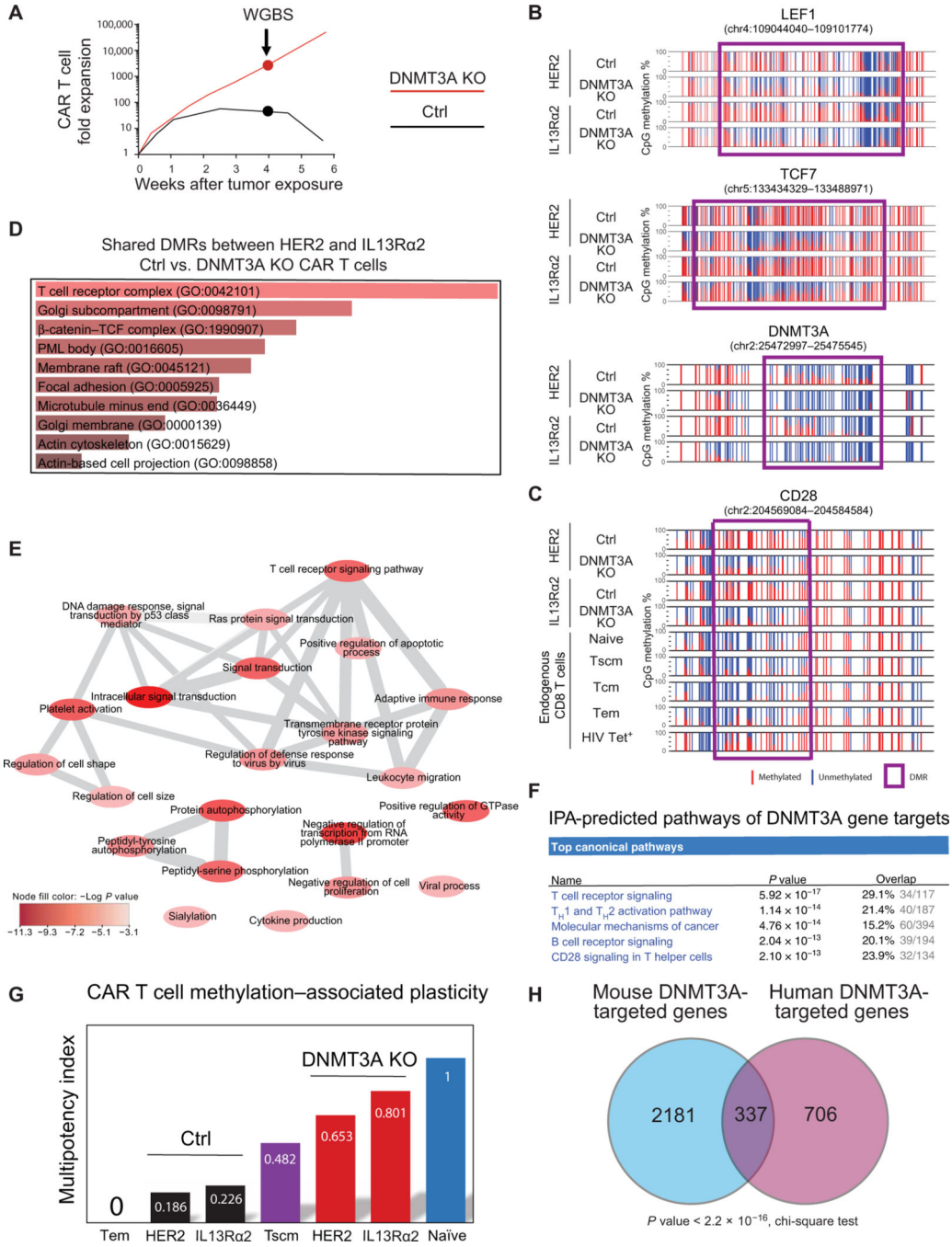

Fig. 3. De novo methylation of T cell plasticity–associated genes is coupled to CAR T cell exhaustion.

(**A**) The experimental design is shown with a representative graph of Ctrl versus DNMT3A KO CAR T cell expansion with subsequent data analysis using samples collected at week 4. Cells were stimulated as described in Fig. 1C. (**B**) WGBS nucleotide- resolution methylation profiling of plasticity-associated signature genes including *LEF1*, *TCF7*, and *DNMT3A* is shown for Ctrl and DNMT3A KO CAR T cells. Individual CpG sites are represented by vertical lines, with red indicating methylation and blue indicating lack of methylation.

Differentially methylated regions (DMRs) are represented by a purple box. (**C**) WGBS methylation profiles are shown for CD28 in Ctrl CAR T cells, DNMT3A KO CAR T cells, and endogenous $CD8^+$ T cell subsets. (**D**) Gene ontology (GO) analysis of DNMT3A-targeted genes is shown. *P* values are based on Fisher's exact test. PML, promyelocytic leukemia nuclear body. (**E**) A graph-based visualization of statistically enriched ($P < 0.001$) nonredundant GO biological processes regulated by DNMT3A-target genes is shown. Color intensity indicates –log *P* value. (**F**) Ingenuity pathway analysis (IPA) predicting the top canonical pathways of DNMT3A gene targets is shown. (**G**) A methylation-based T cell multipotency index (MPI) was used to analyze the whole-genome methylation profiles of IL13Rα2-and HER2-CAR T cells obtained after 4 weeks of repeat stimulation. (**H**) A Venn diagram representation of common versus unique DNMT3A-targeted genes among the current human DNMT3A KO CAR T cell analyses and published LCMV mouse exhaustion studies is shown (15). Of note, only human genes with a mouse homolog were used for the analysis.

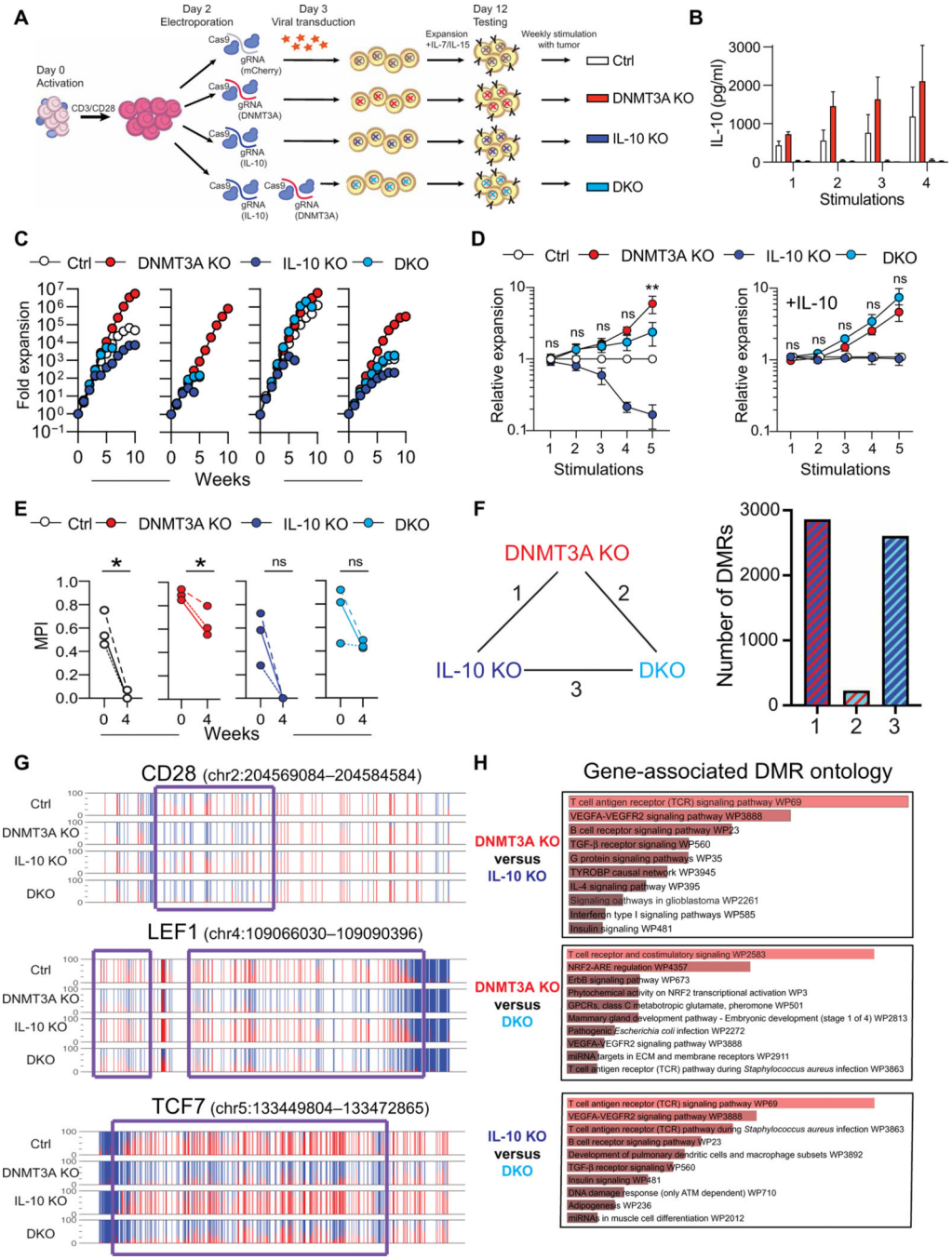

Fig. 4. IL-10 promotes DNMT3A KO CAR T cell survival.

(**A**) Activated human T cells were electroporated with Ctrl (mCherry), DNMT3A, IL-10, or DNMT3A and IL-10 (DKO) RNPs. At day 3, gene-edited T cells were transduced with retroviral vector encoding HER2.ζ-CAR. (**B** to **E**) CAR T cells were incubated with U373 tumor cells at a 2:1 E:T ratio in the presence of exogenous IL-15 and restimulated with fresh tumor cells on a weekly basis until the T cells stopped killing tumor cells. (**B**) Cell culture supernatants were harvested 24 hours after each stimulation, and an IL-10 ELISA was used to determine IL-10 cytokine production. Data are presented as means ± SEM

($n = 5$). (**C**) Gene-edited CAR T cell expansion was measured after weekly stimulations with U373 cells for HER2.ζ-CAR. Each graph represents one healthy donor. (**D**) Left: A summary graph of CAR T cell expansion (relative to Ctrl) for all donors up to five stimulations is shown ($n = 4$ donors). Right: A summary graph of CAR T cell expansion (relative to Ctrl) for all donors in the presence of exogenous IL-10 is shown ($n = 3$ donors). A two-way ANOVA with Sidak's multiple comparisons test was used to compare DNMT3A KO and DNMT3A IL-10 DKO at each stimulation; ns, not significant; $^{**}P < 0.01$. Data are presented as means ± SEM. (**E**) MPIs of Ctrl, IL-10 KO, DNMT3A KO, and DKO CAR T cells were measured before stimulation and after 4 weeks of chronic stimulation ($n = 3$). Data were analyzed by an unpaired *t* test; $^{*}P < 0.05$. Each dot represents data from a single donor. (**F**) The total number of DMRs between week 4 DNMT3A KO (D3A KO), IL-10 KO, and DKO CAR T cells is shown. (**G**) Representative methylation profiles are shown for the *CD28*, *LEF1*, and *TCF7* loci among week 4 Ctrl, DNMT3A KO, IL-10 KO, and DKO CAR T cells. DMRs are represented by a purple box. (**H**) GO analysis of DMRs between week 4 DNMT3A KO, IL-10 KO, and DKO CAR T cells is shown. VEGFA-VEGFR2, vascular endothelial growth factor A–vascular endothelial growth factor receptor 2; GPCRs, G protein–coupled receptors; miRNA, microRNA; ECM, extracellular matrix. TYROBP, protein tyrosine kinase-binding protein; NRF2-ARE, nuclear erythroid 2-related factor 2-antioxidant response element; ATM, ATM Serine/Threonine Kinase.

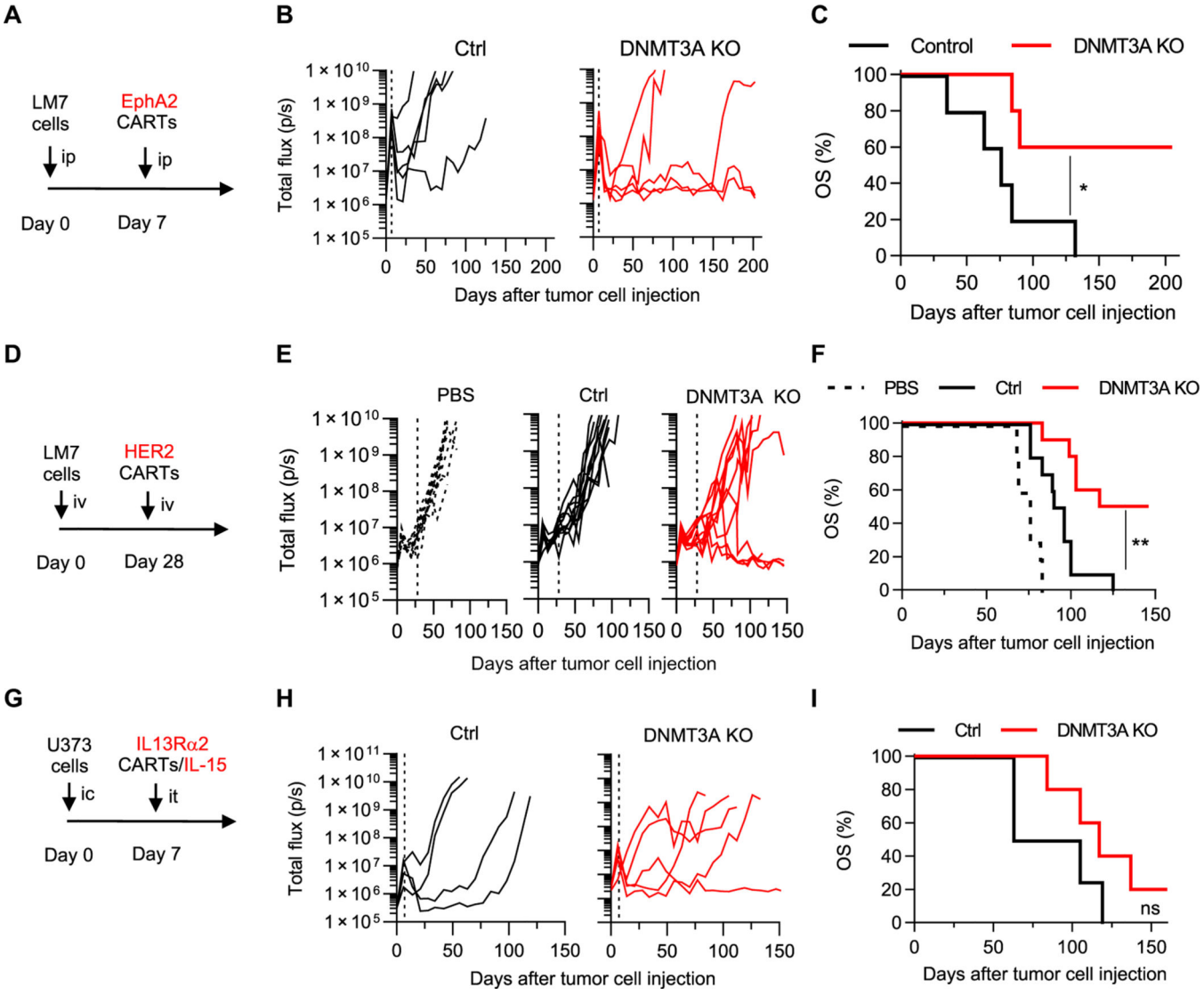

Fig. 5. DNMT3A deletion enhances CAR T cell antitumor activity in vivo.

(**A**) A timeline for the intraperitoneal (ip) LM7 model is shown. NSG mice were injected intraperitoneally with 1×10^6 LM7-ffLuc tumor cells on day 0 and, 7 days later, received a single intraperitoneal dose of 1×10^5 Ctrl or DNMT3A KO EphA2.CD28ζ-CAR T cells (CARTs). (**B**) Quantitative bioluminescence imaging is shown as total flux in photons per second (p/s). The vertical dashed line indicates time of CAR T cell injection. (**C**) A Kaplan-Meier curve shows overall survival (OS) of Ctrl or DNMT3A KO CAR T cell–treated mice ($n = 5$ mice per group). Data were analyzed using a log-rank (Mantel-Cox) test; $^*P < 0.05$. (**D**) A timeline for the intravenous (iv) LM7 model is shown. NSG mice were injected intravenously with 2×10^6 LM7-ffLuc tumor cells and, 28 days later, received a single intravenous dose of 1×10^6 Ctrl or DNMT3A KO HER2.ζ-CAR T cells or PBS. (**E**) Quantitative bioluminescence imaging is shown as total flux. The vertical dashed line indicates time of CAR T cell injection. (**F**) A Kaplan-Meier survival curve is shown ($n = 5$ mice per group). Data were analyzed using a log-rank (Mantel-Cox) test; $^{**}P < 0.01$. (**G**) A timeline for the intracranial (ic) U373 model is shown. NSG mice were injected with 5 ×

10^4 U373-ffLuc tumor cells (intracranially) and, 7 days later, received a single intratumoral (it) dose of 2×10^6 Ctrl or DNMT3A KO IL13Rα2-CAR/IL-15 T cells. (**H**) Quantitative bioluminescence imaging is shown as total flux. The vertical dashed line indicates time of CAR T cell injection. (**I**) A Kaplan-Meier survival curve is shown (Ctrl: $n = 4$ mice, KO: $n = 5$ mice). Data were analyzed using a log-rank (Mantel-Cox) test; ns, not significant.

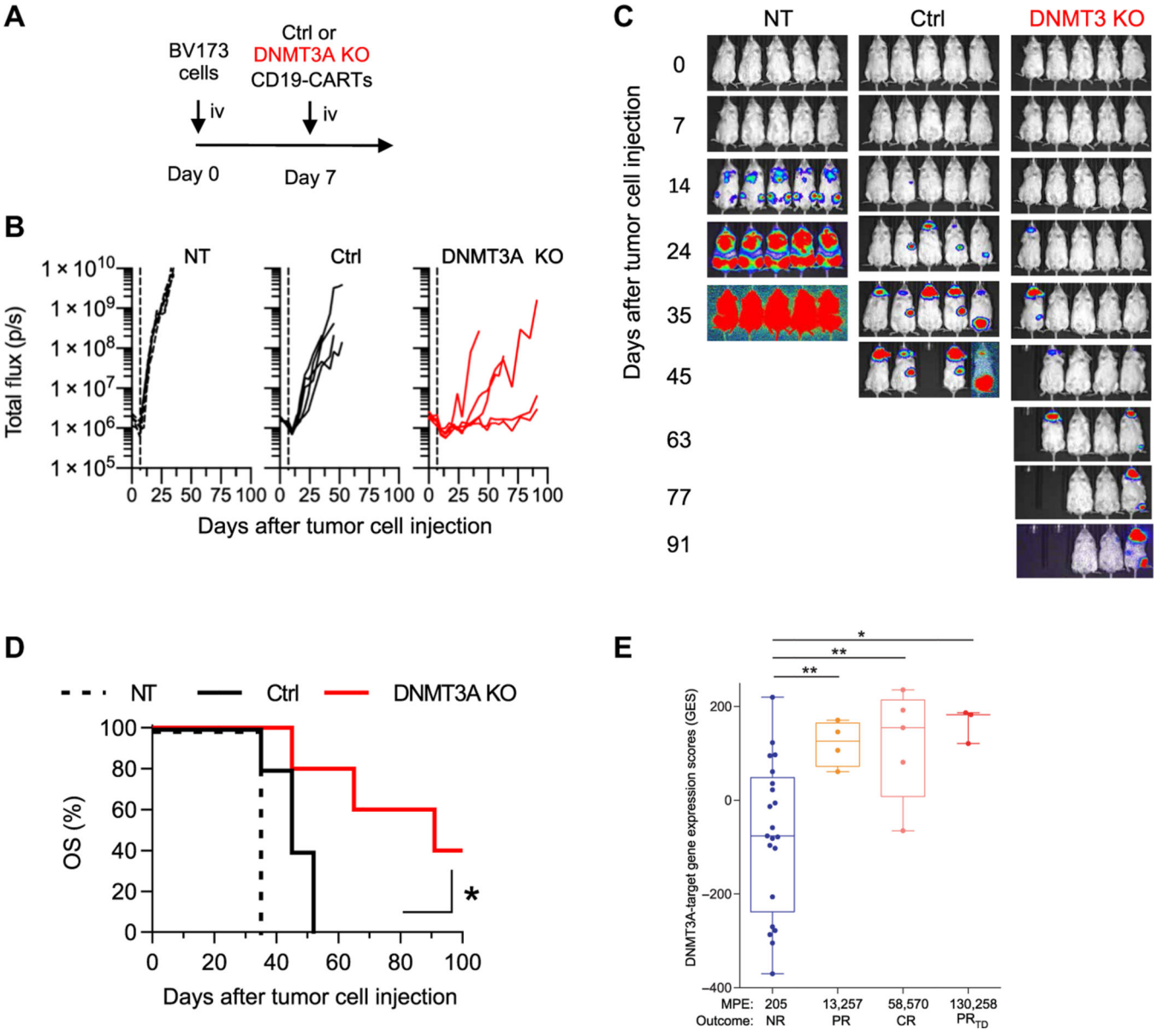

Fig. 6. DNMT3A-mediated gene expression programs regulate CD19-CAR T cell antitumor responses in vivo and predict the clinical outcome.

(**A**) A timeline of intravenous (iv) BV173 model is shown. NSG mice that were injected intravenously with 3×10^6 BV173-ffLuc tumor cells on day 0 received a single intravenous dose of 2×10^6 NT (non-transduced), Ctrl, or DNMT3A KO CD19.41BBζ-CAR T cells 7 days later. (**B**) Quantitative bioluminescence imaging (total flux) data are shown for each mouse. (**C**) Representative bioluminescence images of each treatment group are shown. (**D**) Kaplan-Meier survival curve with log-rank test for significance ($n = 5$ mice per group; $*P < 0.05$). (**E**) DNMT3A-targeted gene expression is shown for CAR T cell products before infusion. Patients were separated on the basis of in vivo expansion and clinical response [NR, nonresponders ($n = 21$); PR, partial responders ($n = 4$); CR, complete responders ($n = 5$); PR_{TD}, PRs followed by relapse with transformed B cell lymphoma ($n = 3$)] after

CD19-CAR T cell infusion for CLL. MPE indicates median peak expansion. Statistical significance was determined by a Mann-Whitney test. Error bars are defined on the basis of the minimum and maximum quartile; $*P < 0.05$ and $**P < 0.01$.